



Control of CRK-RAC1 activity by the *miR-1/206/133* miRNA family is essential for neuromuscular junction function

Ina Klockner¹, Christian Schutt¹, Theresa Gerhardt¹, Thomas Boettger ¹✉ & Thomas Braun ¹✉

Formation and maintenance of neuromuscular junctions (NMJs) are essential for skeletal muscle function, allowing voluntary movements and maintenance of the muscle tone, thereby preventing atrophy. Generation of NMJs depends on the interaction of motor neurons with skeletal muscle fibers, which initiates a cascade of regulatory events that is essential for patterning of acetylcholine receptor (AChR) clusters at specific sites of the sarcolemma. Here, we show that muscle-specific miRNAs of the *miR-1/206/133* family are crucial regulators of a signaling cascade comprising DOK7-CRK-RAC1, which is critical for stabilization and anchoring of postsynaptic AChRs during NMJ development and maintenance. We describe that posttranscriptional repression of CRK by *miR-1/206/133* is essential for balanced activation of RAC1. Failure to adjust RAC1 activity severely compromises NMJ function, causing respiratory failure in neonates and neuromuscular symptoms in adult mice. We conclude that *miR-1/206/133* serve a specific function for NMJs but are dispensable for skeletal muscle development.

¹ Max Planck Institute for Heart- and Lung Research, Department of Cardiac Development and Remodelling, Ludwigstr. 43, D-61231 Bad Nauheim, Germany.
✉email: thomas.boettger@mpi-bn.mpg.de; thomas.braun@mpi-bn.mpg.de

Neuromuscular junctions (NMJs) are chemical synapses, critical for transmitting action potentials from motor neurons to skeletal muscle fibers and initiation of sarcolemma depolarization, eventually resulting in Ca^{2+} release and muscle contraction. The function of NMJs is severely impaired in several neuromuscular diseases such as Congenital Myasthenic Syndromes (CMS), Amyotrophic Lateral Sclerosis (ALS), and Myasthenia Gravis (MG), entailing compromised muscle function, locomotion, and survival¹. Development and maintenance of NMJs require the interaction between motor neurons, terminal Schwann cells, and myofibers, eventually leading to clustering of acetylcholine receptors (AChR), a hallmark of NMJs. Formation of NMJs is initiated by a signaling cascade, involving the receptor tyrosine kinase MuSK, its co-receptor LRP4, and the intracellular Docking Protein 7 (DOK7)^{2,3}. Binding of the presynaptically secreted proteoglycan agrin to postsynaptic LRP4 stimulates MuSK dimerization, phosphorylation, and recruitment of DOK7, thereby sustaining MuSK activity, but also recruiting the adapter proteins CRK and CRK-L^{4,5}. Mutation of *Dok7* (1124_1127dupTGCC), which abolishes binding of CRK/CRK-L to DOK7, causes CMS^{6,7}. Although it was found that expression of both CRK and CRK-L is essential for AChR clustering during NMJ formation^{4,8}, the events downstream of CRK for NMJ formation are not well understood. It has been speculated that CRK might interact with guanine nucleotide exchange factors (GEFs) at the NMJ to stimulate activation of small GTPases but experimental evidence for this hypothesis is lacking^{4,9}.

miRNAs control gene expression at the posttranscriptional level, either by inducing degradation of target mRNAs or by inhibiting their translation¹⁰. Furthermore, miRNAs present in the serum represent useful biomarkers and may serve additional functions in interorgan signaling¹¹. The miRNAs of the *miR-1/206/133* gene family belong to the most abundant miRNAs in striated muscles and are expressed from three separate genomic microRNA clusters. *miR-1/206/133* miRNAs fulfill distinct functions at different developmental stages in the heart as well as in skeletal muscle, which may depend on differential expression of target genes, blockage of putative binding sites, or other reasons^{12–15}. *miR-1* and *miR-133a* are transcribed from two different gene clusters as bi-cistronic pri-miRNA molecules, which are processed to mature *miR-1* and *miR-133a* molecules. *miR-1* and *miR-133a* are co-expressed, since they are derived from a joint pri-miRNA and cooperate to regulate related physiological functions. Deletion of the two genomic *miR-1/133a* clusters revealed a synergistic function of *miR-1/133a* in repressing myocardin and other components of the smooth muscle gene program during early cardiac development¹². Similarly, concomitant deletion of *miR-1-1* and *miR-1-2* activates the smooth muscle gene program in cardiomyocytes and compromises sarcomere formation but does not result in embryonic lethality, confirming synergistic functions of *miR-1* and *miR-133a*¹³. Inactivation of *miR-133a* causes developmental abnormalities due to aberrant cell proliferation and increased smooth muscle gene expression¹⁶. In adult skeletal muscles, *miR-1/133a* is required for metabolic maturation by suppressing the *Dlk1-Dio3* miRNA/lncRNA mega-cluster via MEF2A¹⁴. Surprisingly, however, inactivation of the two *miR-1/133a* gene clusters had no impact on embryonic and postnatal skeletal muscle development, which might be due to compensatory effects of the related *miR-206/133b* miRNA cluster¹⁷ that is specifically expressed in skeletal muscles but not the heart.

Here, we demonstrate that the miRNAs of the *miR-1/206/133* family synergize to play a crucial role in the formation and maintenance of the neuromuscular junction but are dispensable for skeletal muscle development. We discovered that expression of CRK, which is essential for formation and maintenance of

NMJs in skeletal muscles, is adjusted by the concomitant activity of *miR-1/206/133*. Increased expression of CRK enhances its interaction with RAC1-GEF FARP1, thereby boosting activation of the small GTPase RAC1, which prevents formation and maintenance of AChR macro-clusters, essential for NMJ function.

Results

miR-206/133b compensate for *miR-1/133a* in skeletal muscle.

The three miRNA *miR-1/206/133* gene clusters are highly expressed in skeletal muscle^{18,19}. During skeletal muscle development and maturation, the expression of *miR-1*, *miR-133*, and *miR-206* continuously increases, reaching highest levels in adult myofibers. This also holds true for *miR-206*, although the level of *miR-206* declines during postnatal development in whole muscles with a high content of glycolytic fibers, since *miR-206* is most abundantly expressed in oxidative fibers (Supplementary Fig. 1a–c). *miR-1-1* and *miR-1-2* show identical mature microRNA sequences, while the related *miR-206* contains the same seed sequence critical for target binding as *miR-1-1* and *miR-1-2* and differs only by four nucleotides in the rest of the molecule²⁰. Similarly, the mature nucleotide sequences of *miR-133a-1* and *miR-133a-2* are identical and differ from *miR-133b* only by one nucleotide, located outside of the seed sequence (Fig. 1a). The identical seed sequences and overlapping expression profiles of *miR-1-1*, *miR-1-2* and *miR-206* as well as of *miR-133a-1*, *miR-133a-2*, and *miR-133b* strongly suggests overlapping functions¹⁷. This assumption is supported by massive upregulation of *miR-206* in adult skeletal muscle after deletion of *miR-1-1/133a-2//miR-1-2/133a-1* (skeletal muscle-specific *miR-1/133a* double-knockout, dKO)¹⁴. Of note, loss of *miR-1/133a* caused upregulation of *miR-206* in both oxidative and glycolytic muscles, although *miR-206* is only highly expressed in oxidative fibers in wildtype muscles, further arguing for compensatory actions of *miR-206/133b* after loss of *miR-1/133a* (Fig. 1b). On the other hand, it is conceivable that the differences in a few bases in mature *miR-1* and *miR-206*, despite being outside the seed sequences, allow non-overlapping effects of these miRNAs.

To gain insight into the putative cooperative roles of *miR-1/133a* and *miR-206/133b*, we generated skeletal muscle-specific *miR-1/206/133* knockout mice (tKO) by mating *miR-206/133b* sKO to *miR-1/133a* dKO mice^{14,21} (Supplementary Fig. 1d–i). No surviving *miR-1/206/133* tKO mice were observed at weaning (postnatal stage P21) (Fig. 1c, Supplementary table 1a), while germline mutants of *miR-206/133b* (*miR-206/133b* sKO) and *miR-1-1/133a-2^{-/-}//miR-1-2/133a-1^{lox/lox}//Pax7-Cre^{+/-}* (*miR-1/133a* dKO) mice showed the expected Mendelian ratios and no decrease in survival rates. In contrast, *miR-1/206/133* tKO animals delivered by caesarean section at embryonic day 18.5 (E18.5) displayed the expected Mendelian distribution (Fig. 1c, Supplementary table 1b), no gross morphology abnormalities, and no differences in body weight compared to control littermates (Fig. 1d, e). Comparative transcriptome analysis of quadriceps muscles of *miR-1/133a* dKO and *miR-1/206/133* tKO in combination with gene set enrichment analysis (GSEA) revealed a highly significant enrichment of potential *miR-1/206* and *miR-133* target genes in *miR-1/133/206* tKO muscles (Fig. 1f, g). Together with the postnatal lethality of *miR-1/133/206* tKO mice, this observation suggests that the presence of *miR-206/133b* in *miR-1/133a* dKO muscle is sufficient to compensate for the absence of *miR-1/133a* and to repress a large number of *miR-1/133a* target genes. Interestingly, analysis of *miR-1/206/133* tKO mice at E18.5 revealed no signs of increased expression of the *miR-1/133a* target MEF2A, no increase of the expression of the microRNA mega-cluster at the *Dlk1-Dio3* locus, and no mitochondrial dysfunction as previously observed in adult *miR-1/*

a mature microRNA sequence

Chr. 1	miR-206	UGGAAUGUA AAGGAAGUGUGUGG	miR-133b	UUUGGUC CCCUUCAACCAGCUA
Chr. 2	miR-1-1	UGGAAUGUA AAGAAGUAUGUAU	miR-133a-2	UUUGGUC CCCUUCAACCAGCUG
Chr. 18	miR-1-2	UGGAAUGUA AAGAAGUAUGUAU	miR-133a-1	UUUGGUC CCCUUCAACCAGCUG

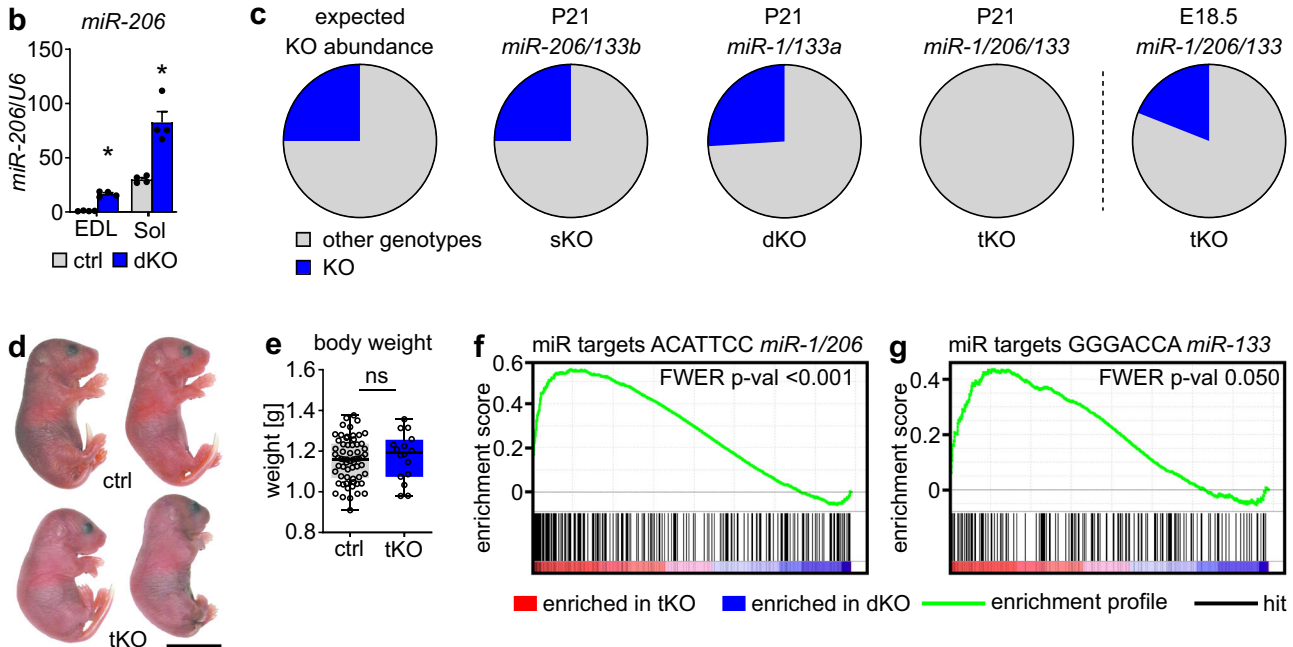


Fig. 1 *miR-206/133b* compensate for the absence of *miR-1/133a* in skeletal muscles to prevent perinatal death. **a** The miRNAs *miR-1*, *-133a/b* and *-206* are encoded in three clusters located on mouse chromosome (Chr.) 1, 2 and 18. The primary sequence of mature *miR-1/133a* is identical; *miR-206* varies from *miR-1* only by four bases, *miR-133b* differs in only one base from *miR-133a* (red). The seed sequence, essential for miRNA-target interaction, is identical in *miR-1/206* and *miR-133a/133b*, respectively (bold blue). **b** Relative expression of *miR-206* in wild-type (control) and adult *miR-1/133a* dKO extensor digitorum longus muscles (EDL) and soleus muscles (Sol) analyzed via TaqMan assay ($n = 4$ ctrl/4 dKO, $n = 4$ ctrl/4 dKO [males/females, 13–17 weeks], Mann-Whitney-U test, one-tailed, $*p = 0.0143$, Data are presented as mean values \pm SEM). *U6 snRNA* served as control. **c** Percentages of *miR-206/133b* sKO and *miR-1/133a* dKO animals at postnatal day 21 (P21) are in accordance to the expected Mendelian distribution (likelihood 25%), while *miR-1/206/133* tKO animals were missing at P21. Analysis of E18.5 animals reveals presence of *miR-1/206/133* tKO animals at this developmental stage (P21: $n = 147$ control littermates 48 sKO, $n = 100$ control littermates/35 dKO, $n = 34$ control littermates/0 tKO at P21; E18.5: $n = 26$ control littermates 6 tKO). **d** Gross morphology of control and *miR-1/206/133* tKO pups after caesarean section (control = littermates, scale-bar: 1 cm [E18.5]). **e** Box-plot of *miR-1/206/133* tKO and control body weight ($n = 63$ control/16 tKO, control = littermates, Mann-Whitney-U test, one-tailed, ns = not significant, Box indicates median and 25th to 75th percentiles, whiskers indicate minimum and maximum [E18.5]). **f, g** GSEA of *miR-1/133/206* tKO compared to *miR-1/133a* dKO quadriceps muscle transcriptome data reveals enrichment of predicted *miR-1/206* and *miR-133* targets in *miR-1/133/206* tKO ($n = 4$ dKO/4 tKO, familywise-error rate method (FWER), $p < 0.001$ (f), $p = 0.05$ (g) [E18.5]). Source data are provided as a Source Data file.

133 dKO mice¹⁴ (Suppl. Fig. 2). We concluded that the function of *miR-1/133a* strongly depends on the developmental stage and that the repression of MEF2A *miR-1/133a* is limited to adult skeletal muscles.

***miR-1/206/133* tKO impairs NMJs but not muscle development.** Most *miR-1/133/206* tKO mutants from heterozygous mutant parents at E18.5 showed only weak movements upon physical stimulation. Furthermore, *miR-1/133/206* tKO mutant lungs mutants failed to float 15 min after caesarean section (Fig. 2a, b), indicating respiratory failure, probably due to the inability of skeletal muscles to expand the lungs. Surprisingly, however, histological analysis did not reveal any obvious changes in skeletal muscle morphology in *miR-1/133/206* tKO mutants at E18.5 (Supplementary Fig. 3a–d). Likewise, the average fiber number and the fiber size distribution were normal in both primarily glycolytic and oxidative muscles (Supplementary Fig. 3e–j) and no substantial alterations in the expression of markers for myogenic development and differentiation were detected in *miR-*

1/206/133 tKO mice (Supplementary Fig. 3k). Ultrastructural analysis by transmission electron microscopy showed well-developed sarcomere structures with clearly visible I-bands and H-zones in skeletal muscles of *miR-1/133/206* tKO mutants that did not deviate from controls (Supplementary Fig. 3l). To investigate potential defects during embryogenesis that might be compensated at later stages of skeletal muscle development, we analyzed *miR-1/206/133* deficient animals at E10.5. We detected no differences in the expression and spatial distribution of Myogenin (*Myog*), a marker of early myogenic differentiation, between *miR-1/206/133* and control animals at E10.5. Identical results were obtained with *miR-1/206/133* germline knock-out animals (gtKO; obtained after mating of *miR-1/133a* constitutive KO¹² to *miR-206/133b* sKO), which were still viable at this stage (Supplementary Fig. 4a).

Next, we tested the ability of primary *miR-1/206/133* tKO muscle stem cells (MuSC) to differentiate in vitro after tamoxifen-induced deletion of *miR-1-2/133a-1* in adult *miR-206/133b*^{-/-}/*miR-1-1/133a-2*^{-/-}/*miR-1-2/133a-1*^{lox/lox}/*Pax7-CreERT2*^{+/-} mice (MuSC tKO, Supplementary Fig. 4b–k). *miR-*

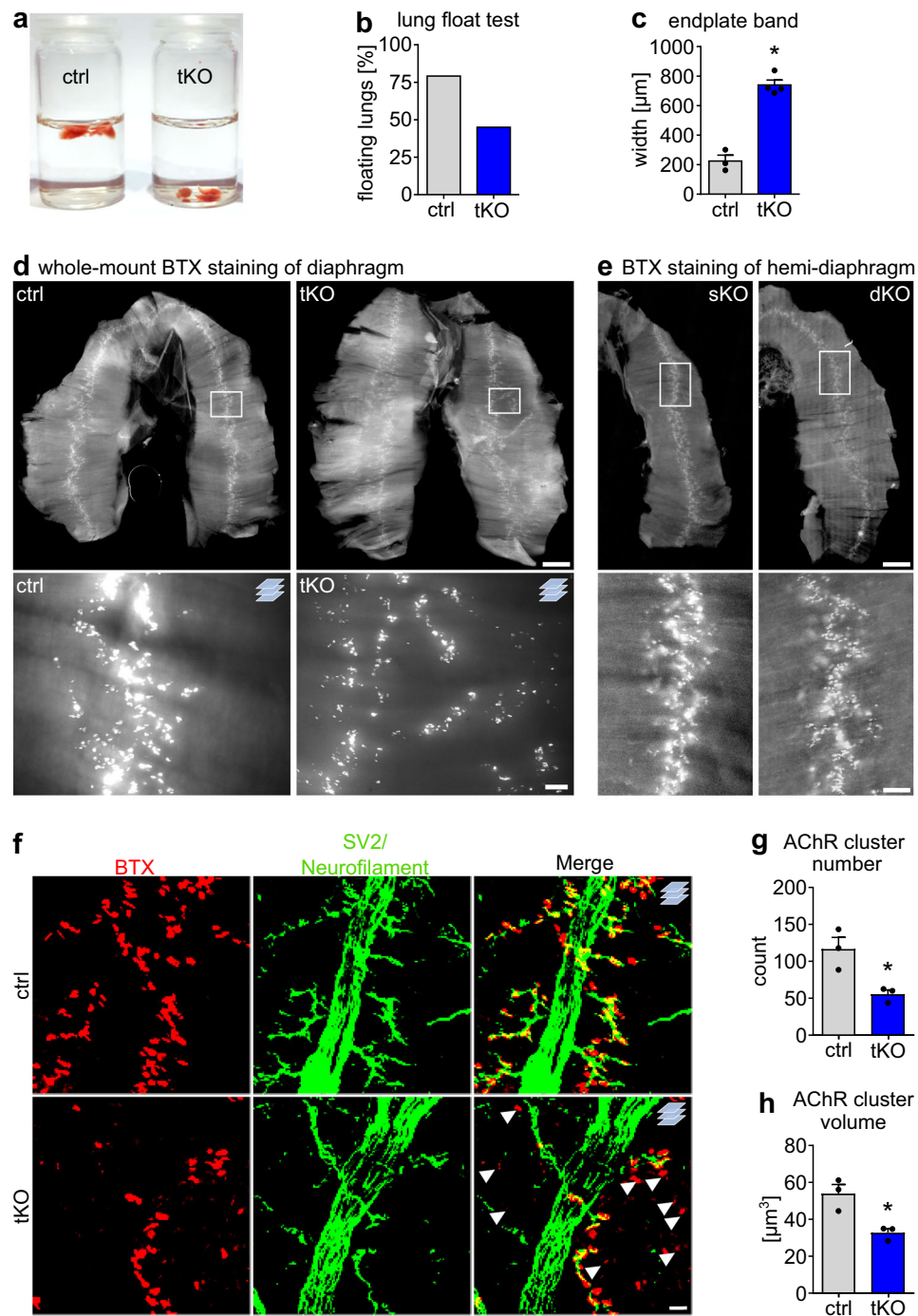


Fig. 2 Loss of *miR-1/206/133* in skeletal muscles disturbs neuromuscular synapse formation and causes respiratory failure. **a** Lung floating test of control and *miR-1/206/133* tKO reveals deficits in breathing after recovery by caesarean section in tKO animals compared to control littermates [E18.5]. **b** Representation of percentages of control and *miR-1/206/133* tKO in the lung floating test (percent of floating lungs in each group; $n = 28$ control/11 tKO from 8 litters, control = littermates [E18.5]). **c** Measurement of average endplate band width of control and *miR-1/206/133* tKO diaphragms ($n = 3$ control/4 tKO, control = littermates, Mann-Whitney-U test, one-tailed, $*p = 0.0286$, [E18.5]). **d** Whole-mount bungarotoxin (BTX) staining of diaphragms from control and *miR-1/206/133* tKO animals (control = littermates, scale-bar: 600 µm upper row/50 µm lower row [50 µm thick Z-stacks lower row, $n = 3$ control/4 tKO, [E18.5]). **e** Whole mount BTX staining of hemi-diaphragms of *miR-206/133b* sKO ($n = 3$) and *miR-1/133a* dKO ($n = 2$) animals (scale-bar: 600 µm upper row/100 µm lower row [E18.5]). **f** Z-stacks of a whole mount-stained diaphragms from control (littermate) and *miR-1/206/133* tKO mice. Anti-SV2 (synaptic vesicles) and anti-neurofilament antibodies were used to label both nerve terminals and axons (green). Staining of the postsynapse was done using BTX (red). Arrows indicate AChR clusters without a nerve terminal in close proximity (scale-bar: 20 µm, $n = 3$ control/3 tKO [E18.5]). **g, h** Quantification of the average AChR cluster number and AChR volume in BTX-stained whole mount diaphragms based on Z-stacks, comparing *miR-1/206/133* tKO and control samples (Supplementary Fig. 5b). Data were obtained from 3D rendered confocal Z-stacks ($n = 3$ control/3 tKO, control = littermates, Mann-Whitney-U test, one-tailed, $*p = 0.05$, [E18.5]). Source data are provided as a Source Data file. Data are presented as mean values +/- SEM in **c** and **g, h**.

1/206/133 tKO and control (*miR-1-1/133a-2^{-/-}//miR-1-2/133a-1^{lox/lox}//miR-206/133b^{-/-}//Pax7-CreERT2^{+/+}*) MuSCs derived from mice with tamoxifen treatment showed the same proliferation rate over 120 h in culture and displayed neither differences in myotube formation nor altered expression of important myogenic factors and other markers of differentiation (Supplementary Fig. 4l–n). Taken together, these results exclude major functions of *miR-1/206/133* for skeletal muscle development, MuSC formation and differentiation.

Since neonatal *miR-1/206/133* tKO mice exhibited normally developed skeletal musculature but only weak movements and eventually died, we wondered whether innervation defects are responsible for the failure to expand the lungs. Therefore, we analyzed innervation of the diaphragm. Whole-mount staining of the diaphragm muscle with Alexa Fluor555-conjugated α -Bungarotoxin (BTX) revealed striking defects in the formation of postsynaptic NMJs in *miR-1/206/133* tKO mice as indicated by dispersed localization of AChR signals (Fig. 2c, d). Furthermore, we detected massive changes in the presynapsis of *miR-1/206/133* tKO diaphragms. Axons were not restricted to a narrow endplate band, but extended to a broader region (Supplementary Fig. 5a). In contrast, *miR-206/133b* sKO and *miR-1/133a* dKO diaphragms displayed a normal pattern of innervation and no alterations of NMJ formation (Fig. 2e). Quantitative analysis of AChR-clusters showed a strong reduction of BTX-stained NMJ endplates in *miR-1/206/133* tKO diaphragm and paraspinal muscles (Fig. 2f, Supplementary Fig. 5b–d). We observed not only a decline of the AChR cluster number (Fig. 2g), but also a significant reduction of the AChR cluster size in both diaphragm and paraspinal muscles (Fig. 2h, Supplementary Fig. 5e–f). In agreement with the morphological assessment, transcriptome data of synaptic marker genes indicated an upregulation of key postsynaptic molecules (Supplementary Fig. 5g) and GSEA unveiled a highly significant enrichment of gene sets associated with neuromuscular synapse formation and assembly in *miR-1/206/133* tKO quadriceps muscles (Fig. 3a–c). We reasoned that the increased expression of synaptic genes represents a secondary effect due to reduced innervation of tKO muscle^{22,23}. We concluded that the loss of all *miR-1/206/133* clusters impairs formation of NMJs but otherwise has no discernible effects on myofiber differentiation.

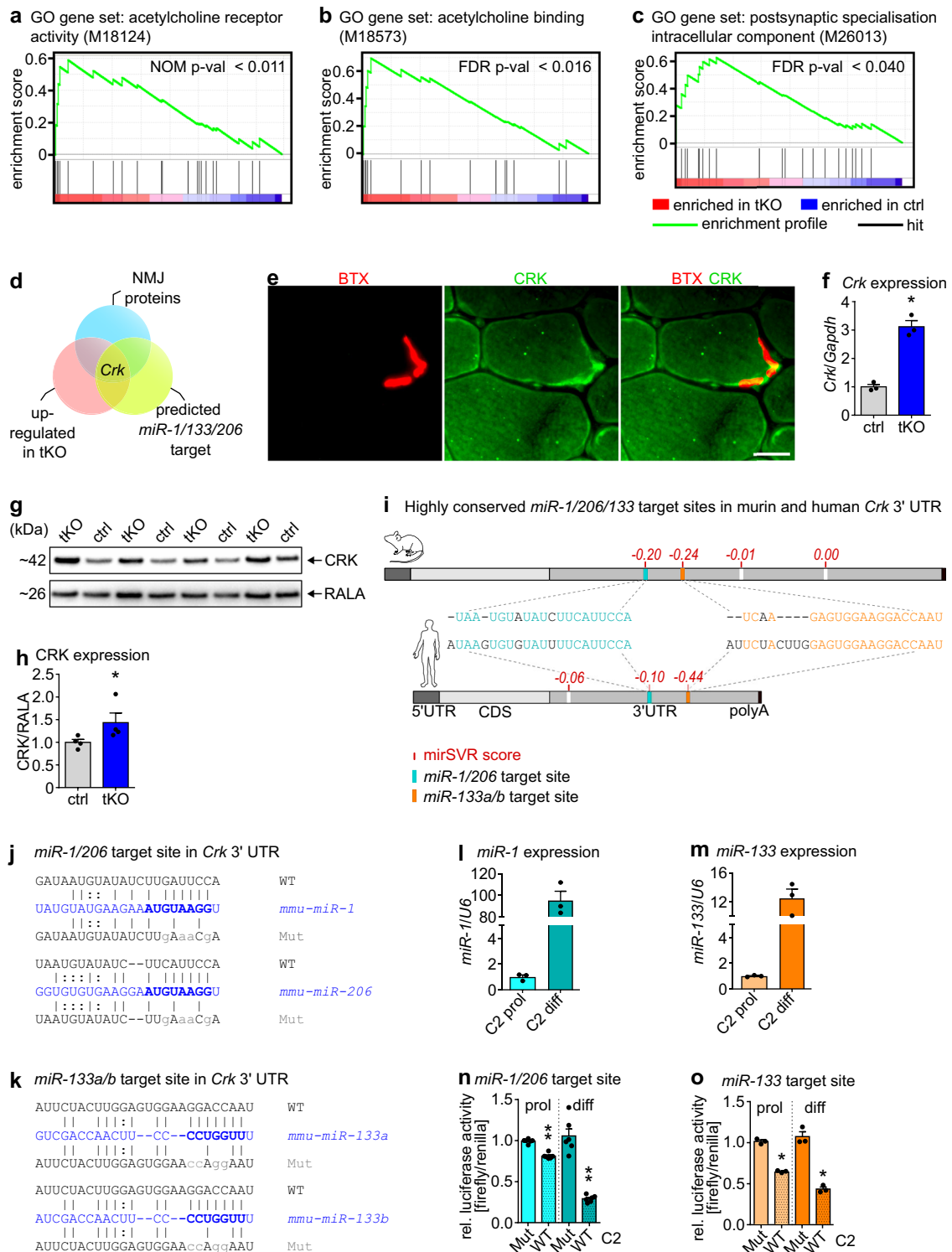
***miR-1/206/133* adjust the concentration of CRK at NMJs.** To identify primary targets of *miR-1/206/133* and thereby gain insight into the molecular mechanism by which these miRNAs control NMJ formation, we analyzed the overlap of *miR-1/206/133* tKO transcriptome data, predicted *miR-1/206/133* target genes, and known NMJ-associated genes. *Crk* emerged out of this analysis as a potentially relevant primary *miR-1/206/133* target (Fig. 3d, Supplementary table 2). CRK is an adapter protein that is ubiquitously expressed and fulfills important roles in several signaling pathways by mediating signaling events downstream of receptor tyrosine kinases^{24–26}. In skeletal muscle, CRK and CRK-L play a critical role during formation of neuromuscular synapses downstream of the MuSK-binding protein DOK7^{4,7,8}. Interestingly, CRK was specifically enriched at NMJs in myofibers (Fig. 3e)⁴ and even more importantly, inactivation of *miR-1/206/133* caused a profound increase of CRK mRNA and protein levels in skeletal muscles (Fig. 3f–h). Inspection of the nucleotide sequence of CRK uncovered target sites for *miR-1/206* and *miR-133* in the 3'-UTR of murine *Crk* mRNA, which were highly conserved in human *Crk* (Fig. 3i). To confirm the putative repression of *Crk* by *miR-1/206/133*, we studied the functional relevance of the most strongly conserved *miR-1/206* and *miR-133* target sites using luciferase reporter assays in C2 myoblasts and myotubes (Fig. 3j, k). After transfection of the luciferase reporter

constructs, cell lysates were prepared from either proliferating myoblasts or differentiating myotubes, since myoblasts express much lower amounts of *miR-1/133* than differentiated myotubes (Fig. 3l, m)^{14,19,27}. In line with the potential repression of *Crk* by *miR-1/206/133*, activity of the luciferase reporter was much lower in proliferating than in differentiated myotubes. The reduction of luciferase reporter activity in myoblast compared to myotubes was not apparent anymore when the predicted miRNAs target sites were mutated (Fig. 3n, o), suggesting that endogenous levels of *miR-1/206/133* mediate repression of *Crk* in myotubes.

High CRK activates RAC1 via FARP1, disturbing NMJ function. Previous studies reported a role of CRK downstream of LRP4/MuSK/DOK7, probably by recruitment of GEFs (guanine nucleotide exchange factors) to NMJs^{4,28}, which might be instrumental for activation of small GTPases such as RAC and RHO. Since these small GTPases are essential for formation of agrin-induced AChR-micro- and macro-clusters in vitro^{29,30}, we wondered whether CRK is the missing link that connects MuSK with RAC or RHO activation⁹. Immunoprecipitation of CRK followed by mass spectrometry revealed an interaction of CRK with the RAC1-GEF FARP1³¹. The amount of co-immunoprecipitated FARP1 was higher in E18.5 *miR-1/206/133* tKO limb muscles compared to WT (Suppl. Fig. 6a–c), suggesting that loss of *miR-1/206/133* increases CRK-FARP1 interactions leading to enhanced RAC1 activity. To confirm enhanced interaction of CRK and FARP1 in *miR-1/206/133* tKO muscle, we performed proximity ligation assays (PLA) using myofibers differentiated from control and *miR-1/206/133* deficient MuSCs (MuSC *miR-1/206/133* tKO). The PLA assay detected increased amounts of endogenous CRK in close proximity to the RAC1-GEF FARP1 in differentiated *miR-1/206/133* tKO muscle fibers (Supplementary Fig. 6d–f). The interaction of CRK with FARP1 was validated by co-immunoprecipitation using a FARP1 antibody again (Supplementary Fig. 6g). In addition, mass spectrometry-based proteomics of control and *miR-1/206/133* tKO quadriceps muscles revealed enrichment of RAC GTPase binding proteins in *miR-1/206/133* tKO muscles (Fig. 4a, Supplementary Fig. 6h, i). We also observed enhanced RAC-GTP downstream signaling at the transcriptional level via GSEA in *miR-1/206/133* tKO muscles (Supplementary Fig. 7a, b), which corroborates that loss of *miR-1/206/133* and the subsequent rise in CRK increases activity of small GTPases in *miR-1/206/133* tKO muscles. While expression levels of *miR-1/206/133* have an instructive role for AChR-clustering, agrin-induced AChR clustering does not affect expression of *miR-1/206/133* (Supplementary Fig. 8a–c).

To explore in more detail the impact of increased CRK levels on RAC1 GTPase activity, we performed pull down assays for active RAC1 (RAC1-GTP). Forced expression of CRK in C2 cells strongly activated RAC1 in myotubes (Fig. 4b) and impaired formation of agrin-induced AChR-macro-clusters (Fig. 4c, d), indicating that the amount of CRK needs to be tightly regulated for achieving the appropriate degree of RAC1 activation. In contrast, increased expression of the CRK paralog CRK-L did not affect AChR formation, showing the same lack of effects as control transfections (Supplementary Fig. 8d–g). Similar to *Crk* transfections, expression of a constitutive active version of RAC1 (RAC^{G12V}) also impaired AChR-macro-cluster formation (Fig. 4e, f)³⁰, further demonstrating that increased levels of CRK enhance recruitment of FARP1 to forming AChR-macro-clusters leading to overactivation of RAC1, which impairs AChR-macro-cluster formation in vitro.

Forced *Crk* expression disrupts NMJ formation in vivo. To explore whether loss of *miR-1/206/133*-mediated repression of CRK is sufficient to disturb formation of NMJ, we overexpressed CRK in



skeletal muscles *in vivo* in transgenic mice. Due to the anticipated lethality of CRK overexpression, we recovered 61 animals at E18.5, which were injected at the pronuclear stage with a CRK-construct under control of a skeletal muscle-specific promoter³². The 3'-UTR containing the *miR-1/206/133* target sequences was not included to avoid counter-regulation by *miR-1/206/133*. 16% of injected animals carried the transgene (*Crk-tg*) (Fig. 5a, Supplementary Fig. 9a) and expressed varying concentrations of CRK in skeletal muscles as measured by western blot analysis (Fig. 5b, c). We also created a second mouse model of *Crk* overexpression, based on the CRISPR-

dCas9-SPH system³³, to enable temporally controlled over-expression of *Crk* in embryonic and adult skeletal muscles after activation by skeletal muscle-specific expression of Cre-recombinase. sgRNAs targeting the transcriptional start site of *Crk*³⁴ were tested in C2 myoblasts using the dCAS9-VPH system³⁵. The most effective sgRNA (Fig. 5d) was selected to generate U6-sgRNA transgenic mice. *U6-sgRNA*^{+/-}//*Pax7-ICN-Cre*^{+/-}//*CAG-LSL-dCas9-SPH*^{+/-} (*Crk-SPH*) mice (Fig. 5e, Suppl. Fig. 9b-d), showing dCas9-SPH activity and massively increased *Crk* expression in skeletal muscles (Fig. 5f, g), were recovered at E18.5. Importantly, we observed

Fig. 3 The NMJ associated adapter protein Crk contains evolutionary conserved miR-target sites in the 3' UTR and is a target for miR-1/206/133. **a–c** GSEA of control and *miR-1/206/133* tKO quadriceps muscle transcriptome data ($n = 4$ control/4 tKO, control = *miR-1-1/133a-2^{+/+}/miR-1-2/133a-1^{lox/lox}/miR-206/133b^{+/+}/Pax7-Cre^{+/+}*, familywise-error-rate method (FWER), $p = <0.011$ (**a**), $p = <0.016$ (**b**), $p = <0.040$ (**c**) [E18.5]). GO = Gene Ontology. **d** Overlap of transcriptome data (significantly up-regulated in tKO with fold change >1.35) and predicted *miR-1/206/133* target genes identified the NMJ-associated gene *Crk* as a top candidate. **e** CRK immunostaining reveals localization at the postsynapse in transversal sections of WT TA-muscles (scale-bar: 20 μm , BTX = bungarotoxin, $n = 2$ [male, 14 weeks]). **f** *Crk* expression in *miR-1/206/133* tKO deficient muscles compared to control quadriceps (TaqMan assay, $n = 3$ control/3 tKO, control = *miR-1-1/133a-2^{+/+}/miR-1-2/133a-1^{lox/lox}/miR-206/133b^{+/+}/Pax7-Cre^{+/+}*, Mann-Whitney-U test, one-tailed, $*p = 0.05$, [E18.5]). *Gapdh* served as control. **g, h** Western blot analysis of CRK expression in *miR-1/206/133* deficient diaphragm muscles (tKO) compared to control. RALA served as control. ($n = 4$ control/4 tKO, control = *miR-1-1/133a-2^{+/+}/miR-1-2/133a-1^{lox/lox}/miR-206/133b^{+/+}/Pax7-Cre^{+/+}*, Mann-Whitney-U test, one-tailed, $*p = 0.0143$, [E18.5]). **i** Conserved predicted binding sites in murine and human *Crk* mRNA. Putative *miR-1/206* target sites (turquoise) and *miR-133* binding sites (orange) in the 3' UTR. MicroRNA target sites ranked by mirSVR down-regulation score (red). CDS = coding sequence, UTR = untranslated region, polyA = polyadenylation-tail. **j, k** WT and mutated (Mut) sequences (gray) of putative *miR-1/206* (**j**) and *miR-133a/b* (**k**) target sites in the 3' UTR of *Crk* were cloned into luciferase reporter vectors. MiR-sequence (blue), seed-sequence (bold blue). **l, m** Endogenous *miR-1* or *miR-133* expression in proliferating (prol) and differentiation stages (diff) of C2 cells (TaqMan assays, $n = 3$ prol/3 diff, $n = 3$ prol/3 diff, biological replicates). *U6* served as control. **n, o** Repression of firefly-luciferase activity in Dual-Luciferase reporter assays by WT but not mutated (Mut) *miR-1* or *miR-133* miRNA target sites from 3' UTR of *Crk*. Repression of firefly-luciferase by the respective WT target sites is detected in proliferating, but is more pronounced in differentiating (diff) C2 cells (*miR-1/206* target site $n = 6$ Mut/6 WT, *miR-133* target site $n = 3$ Mut/3 WT, biological replicate = independent transfection, Mann-Whitney-U test, one-tailed, $**p = 0.0011$, $*p = 0.05$). Normalization via renilla-luciferase (endogenous control). Source data are provided as a Source Data file. Data are presented as mean values \pm SEM in **f–h** and **l–o**.

disturbed distribution of BTX-positive postsynaptic AChR-clusters in the diaphragm of both the *Crk-tg* and the *Crk-SPH* models at E18.5, very similar to the *miR-1/206/133* tKO phenotype. Not only the distribution of AChR-clusters was much more dispersed (Fig. 5h), but also the AChR cluster number was strongly reduced (Fig. 5i). Consistent with the severe impairment of postsynaptic development, *Crk-SPH* mice did not survive early postnatal development but similar to *miR-1/206/133* tKO animals presented with normal body weight and normal gross morphology at E18.5 (Fig. 5j–l; Supplementary Table 3). GSEA of transcriptome data of *Crk*-overexpressing animals compared to littermates revealed enrichment of gene sets associated with synapse assembly and function (Fig. 5m, n). Likewise, expression of FARP1 was increased in *Crk-SPH* mice (Supplementary Fig. 6i), further supporting the relevance of the CRK-FARP1-RAC1 in formation of NMJs. Taken together, recapitulation of the *miR-1/206/133* tKO phenotype in two independent models of increased *Crk* expression strongly suggests that tight control of the adaptor protein CRK is a crucial function of *miR-1/206/133* during early postnatal skeletal muscle development to achieve proper NMJ formation.

Maintenance of NMJ depends on *miR-1/206/133* in adult muscles. Our finding that *miR-1/206/133* tKO mice at E18.5 do not show increased expression of the microRNA mega-cluster at the *Dlk1-Dio3* locus and mitochondrial dysfunction as adult *miR-1/133* dKO mice¹⁴, strongly suggest that the function of *miR-1/133a* depends on the developmental stage. Thus, we decided to interrogate the potential redundancy of *miR-206/133b* with *miR-1/133a* miRNAs and the role of *miR-1/206/133* for NMJ maintenance in adult skeletal muscles. To accomplish efficient deletion of *miR-1/206/133* in adult skeletal myofibers, we used *HSA-rtTA/TRE-Cre* mice³⁶ in combination with the *miR-206/133b^{-/-}/miR-1-1/133a-2^{-/-}/miR-1-2/133a-1^{lox/lox}* strain (adult *miR-1/206/133* tKO). Efficiency of Cre-recombination was verified by doxycycline treatment of *HSA-rtTA/TRE-Cre^{+/+}/Z/AP-Cre^{+/+}* reporter mice for three weeks (Supplementary Fig. 10a)³⁷, which was sufficient to achieve complete recombination of the reporter construct in skeletal muscle fibers (Supplementary Fig. 10b). TaqMan analysis confirmed a strong reduction of *miR-1/133a* expression in TA and soleus muscles of adult *miR-1/206/133* tKO mice nine weeks after starting the three weeks doxycycline treatment (Fig. 6a–e). Furthermore, we repeated the doxycycline treatment regimens every six weeks to ensure that new nuclei contributed by fusing myoblasts will also undergo recombination. Expression analysis by Affymetrix

microarray and TaqMan analyses of adult *miR-1/206/133* tKO skeletal muscles revealed a strong enrichment of *miR-1* and *miR-133* target gene sets in skeletal muscle 28 weeks after initiation of doxycycline administration (Fig. 6f, g), including upregulation of *Crk* (Fig. 6h). Consistent with observations in neonatal *miR-1/206/133* tKO mice, we also observed activation of RAC1 downstream signaling in adult *miR-1/206/133* tKO animals by transcriptional profiling and GSEA (Supplementary Fig. 11a, b). To directly compare adult *miR-1/206/133* tKO animals to mice expressing increased levels of CRK in myofibers, we generated adult *Crk-SPH* mice (*U6-sgRNA^{+/-}/HSA-rtTA/TRE-Cre^{+/+}/CAG-LSL-dCas9-SPH^{+/-}*) allowing doxycycline-dependent control of *Crk* expression (Fig. 6i). Western blot analysis confirmed strongly increased CRK levels in skeletal muscles of adult *Crk-SPH* mice, one week after completion of the 3-weeks long doxycycline treatment (Fig. 6j). Overexpression of CRK in adult skeletal muscles led to activation of RAC1 downstream targets, such as PAK1/2/3, corroborating elevated RAC1 activity in response to increased CRK expression (Supplementary Fig. 11c–e).

Importantly, both adult *miR-1/206/133* tKO and adult *Crk-SPH* mice displayed severe and progressive deficits in motor function, which in case of adult *Crk-SPH* mice became already apparent one week after completion of the doxycycline treatment. We observed muscle weakness, abnormal hindlimb clasp after lifting mice at the tail, and massive disturbance of limb coordination as indicated by footprint assays (Fig. 7a)^{38–40}. Similarly, adult *miR-1/206/133* tKO and adult *Crk-SPH* mice showed reduced performance in Rotarod tests (Fig. 7b–e)^{38,41}. In line with these findings, molecular analysis revealed strong enrichment of gene sets involved in organization of the postsynapse in skeletal muscles of adult *miR-1/206/133* tKO mice (Fig. 7f, g). Of note, deficits in motor function were not apparent in adult *miR-1/133a* dKO and *miR-206/133b* KO mice (Supplementary Fig. 12a–c, Fig. 7a), while adult *miR-1/206/133* tKO showed the same upregulation of microRNA mega-cluster at the *Dlk1-Dio3* locus and mitochondrial dysfunction as adult *miR-1/133a* dKO (Supplementary Fig. 13). Impaired neuromuscular functions corresponded well to morphological changes of postsynaptic NMJ regions in skeletal muscles. We detected a significant decrease of the number of BTX-stained postsynaptic NMJ regions in adult *miR-1/206/133* tKOs and adult *Crk-SPH* animals. Furthermore, we observed fragmentation of pretzel-shaped branches of AChR clusters in isolated single fibers as well as in whole muscle preparations (Fig. 7h–j, Supplementary Fig. 14). Taken together, these results indicate that adjustment of CRK-levels

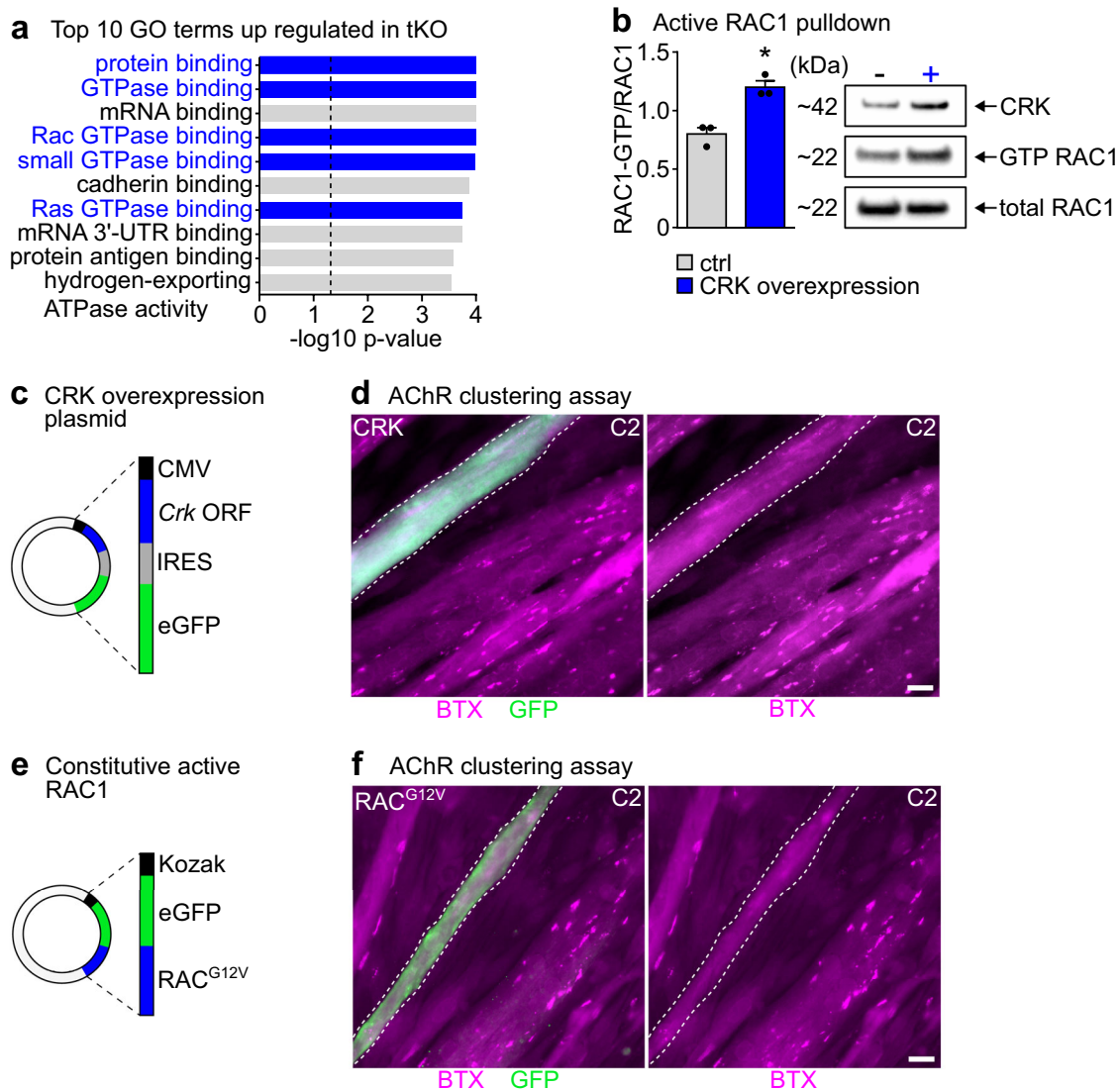


Fig. 4 Increased levels of CRK in skeletal muscle cells activate RAC1, resulting in impaired AChR clustering. **a** Top 10 up regulated GO (Gene Ontology) terms of molecular function in Proteome data indicate increased small GTPase activity (terms labelled in blue) in *miR-1/206/133* tKO vs. WT proteome obtained from Quadriceps muscles at E18.5 ($n = 3$ WT/3 tKO). **b** Active RAC1 pull-down assays exhibit significant increase of RAC1 activation (RAC1-GTP) upon CRK overexpression in skeletal muscle cells ($n = 3/3$ independent transfections and pull-down assays, loaded on three gels, Mann-Whitney-U test, one-tailed, $*p = 0.05$). Data are presented as mean values \pm SEM. RAC1-GTP levels were normalized to total RAC1 levels using Western blot analysis. **c, d** *Crk* was ectopically expressed in C2 myotubes using a vector with CMV promoter and IRESII-mediated GFP co-expression (**c**). Transfected myotubes were incubated with agrin to induce AChR clustering. GFP-positive (anti-GFP-Alexa488), *Crk*-overexpressing myotubes loose BTX-positive AChR-macro-clusters (stained by Alexa Fluor594-conjugated BTX; scale-bar: 20 μ m). Dashed lines mark myotubes expressing *Crk*-GFP (**c**) and *RAC1*^{G12V}-GFP (**d**). Minimum $n = 6$ (biological replicate = independent transfection). **e, f** Constitutive active RAC1 (*RAC1*^{G12V}) was ectopically expressed in C2 myotubes. Transfected myotubes were treated with agrin to induce AChR clustering. *RAC1*^{G12V}-GFP (Alexa488) positive myotubes loose AChR-macro-clusters (stained by Alexa Fluor594-conjugated BTX; scale-bar: 20 μ m). Minimum $n = 6$ (biological replicate = independent transfection). Source data are provided as a Source Data file.

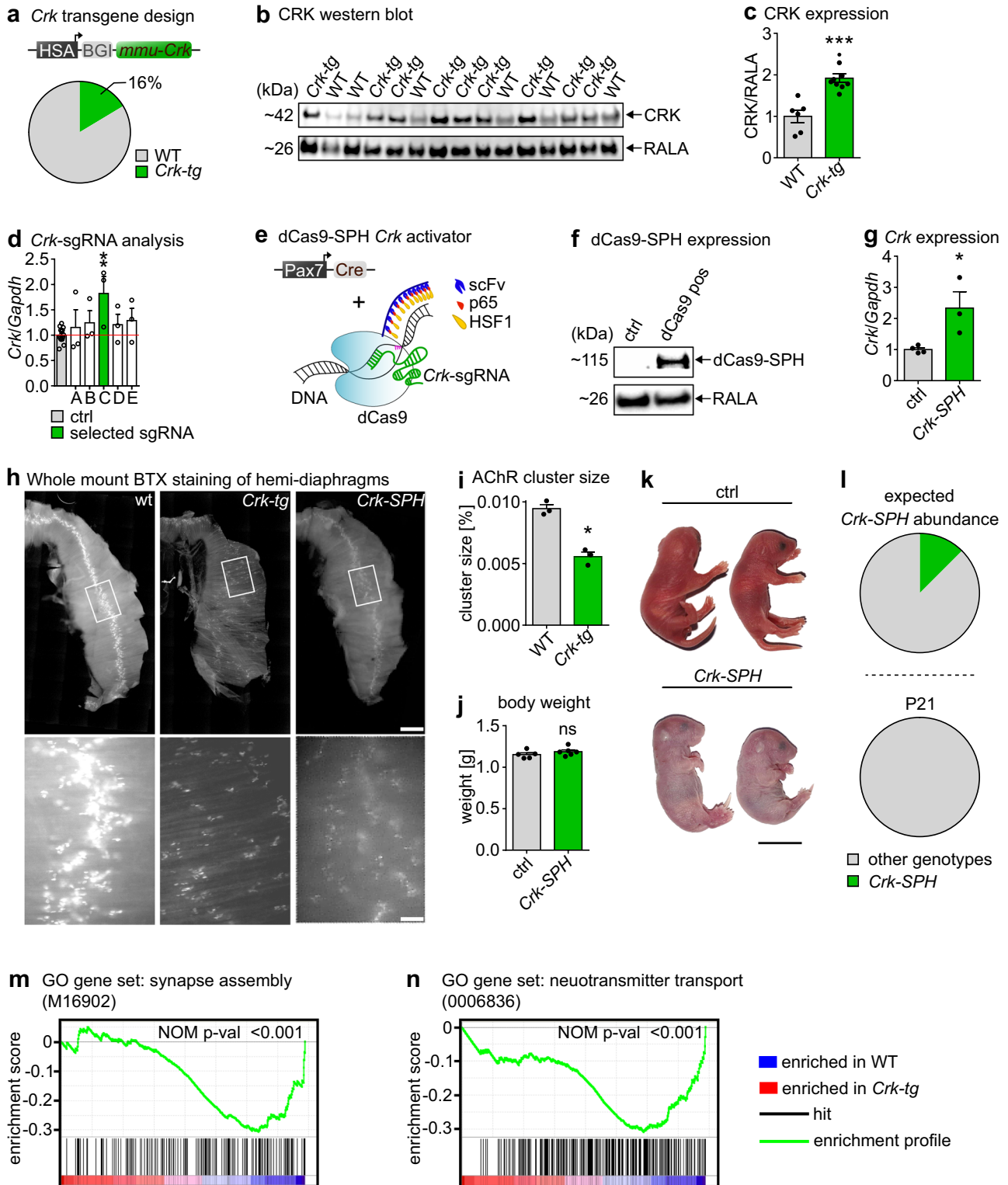
by *miR-1/206/133* is not only essential for NMJ formation but also critical for maintaining neuromuscular functions in adult mice, probably by controlling RAC1 activity via limiting recruitment of FARP1 to NMJs (Fig. 8). Surprisingly, this pivotal mechanism, necessary for enabling locomotion, depends on the combined activity of three *miR-1/206/133* gene clusters.

Discussion

Here we demonstrate that CRK levels in skeletal muscle myofibers need adjustment by *miR-1/206/133*-mediated posttranscriptional regulation to establish the necessary degree of localized RAC1 activity required for NMJ formation and maintenance. Our study

reveals that *miR-1/206/133* are instrumental to customize expression of the ubiquitous adapter protein CRK to the needs of myofibers, thereby enabling proper AChR clustering. Furthermore, we show that CRK is the missing link that connects the LRP4-MuSK-DOK7 signaling complex to localized RAC1 activity at newly forming AChR-clusters by recruitment of GEF FARP1, eventually enabling formation of functional NMJs. This signaling mechanism is not only critical for postsynaptic NMJ development but also indispensable for maintenance of NMJs in adult skeletal muscles.

CRK is a universal adapter protein, essential for several signaling pathways in different cell types^{42,43}, which also serves specific functions for NMJ formation in skeletal muscles together



with its paralog CRK-L⁴. Previous work based on loss-of-function approaches revealed that NMJ formation requires the presence of CRK and CRK-L, but did not appreciate the necessity to adjust CRK levels in a relatively narrow range. We found that post-transcriptional repression of CRK by *miR-1/206/133* is necessary to avoid detrimental effects on NMJ formation caused by increased levels of CRK. It was known that CRK acts downstream of the LRP4/MuSK/DOK7 signaling complex, but effects mediated by CRK were unclear². We found that CRK interacts with

FARP1 probably via its SH3 (Src homology 3) domain, which acts as a recognition site for proline-rich motifs of several interaction partners^{26,44}. In addition, CRK contains a SH2 (Src homology 2) domain that allows binding to DOK7^{4,7,45}. CRK was recently reported to interact not only with DOK7 but also directly with the tyrosine-phosphorylated JM region of MuSK. This redundancy of CRK recruitment highlights the importance of balanced CRK levels at NMJs⁴⁵. FARP1 is known as a GEF, stimulating RAC1 activity in neuronal postsynaptic spines downstream of SynCAM

Fig. 5 Forced expression of *Crk* in skeletal muscles recapitulates the *miR-1/206/133* knock-out phenotype. **a** Muscle-specific *Crk* overexpression by the HSA-promoter. 16% of all obtained animals were transgene-positive tested ($n = 51$ WT/10 *Crk-tg* [E18.5]). **b, c** Increased CRK levels in *Crk-tg* quadriceps muscles. RALA served as loading control (Western blot, $n = 6$ WT/9 *Crk-tg*, WT = littermates, Mann-Whitney-U test, two-tailed, $***p = 0.0004$ [E18.5]). **d** Co-transfection of SP-dCas9-VPR64 vector and sgRNA vectors for *Crk* activation in C2 cells. Selected sgRNA C (green) for further analysis (TaqMan assay, control = transfections of unrelated sgRNAs $n = 15$, sgRNAs A-E tested in independent transfections $n = 3$, Mann-Whitney-U test, one-tailed, $**p = 0.0049$). *Gapdh* served as control. **e** *Pax7-Cre*-driven dCas9-SPH³³ activation system with selected *Crk*-sgRNA. **f** *Pax7-Cre*-dependent dCas9-SPH expression in quadriceps muscles of *Pax7-Cre^{+/-}//CAG-LSL-dCas9-SPH^{+/-}* mice (Western blot, $n = 3$ control/3 *Crk-SPH*, control = *sgRNA^{+/+}* [E18.5]). RALA served as control. **g** Increased expression of *Crk* in quadriceps muscle using the *Pax7-Cre*-dependent dCas9-SPH system in combination with *Crk*-sgRNA expression compared to control (TaqMan assay, $n = 4$ control/3 *Crk-SPH*, control = *sgRNA^{+/+}*, Mann-Whitney-U test, one-tailed, $*p = 0.0286$ [E18.5]). *Gapdh* served as control. **h** Whole-mount bungarotoxin (BTX) staining of hemi-diaphragms of *Crk* overexpressing *Crk-tg* ($n = 9$) and *Crk-SPH* ($n = 3$) animals compared to WT (scale-bar: 600 μ m/100 μ m [E18.5]). **i** Mean AChR cluster size in paraspinal muscles on transversal sections of WT ($n = 3$) and *Crk-tg* ($n = 3$) animals (WT = littermates, Mann-Whitney-U test, one-tailed, $*p = 0.05$ [E18.5]). **j** Body weight of control ($n = 5$) and *Crk-SPH* ($n = 6$) pups (control = *sgRNA^{+/+}* littermates, Mann-Whitney-U test, one-tailed, ns = not significant [E18.5]). **k** Morphology of control and *Crk-SPH* pups; *Crk-SPH* animals appeared cyanotic (control = *sgRNA^{+/+}* littermates, scale-bar: 1 cm [E18.5]). **l** Percentages of *Crk-SPH* animals at postnatal day 21 (P21) correspond to expected Mendelian ratios (likelihood 12.5%). *Crk-SPH* genotype (*sgRNA^{+/-}//dCas9^{+/-}//Pax7-Cre^{+/-}*) is absent at P21 ($n = 38$ control/0 *Crk-SPH*; control = littermates). **m, n** GSEA of control ($n = 3$) vs. *Crk-tg* ($n = 3$) quadriceps muscles transcriptome data (WT = littermates, Nominal p -value (NOM p -val), $p = 0.000$ (m, n) [E18.5]). Source data are provided as a Source Data file. Data are presented as mean values \pm SEM in **c, d, g** and **l, j**.

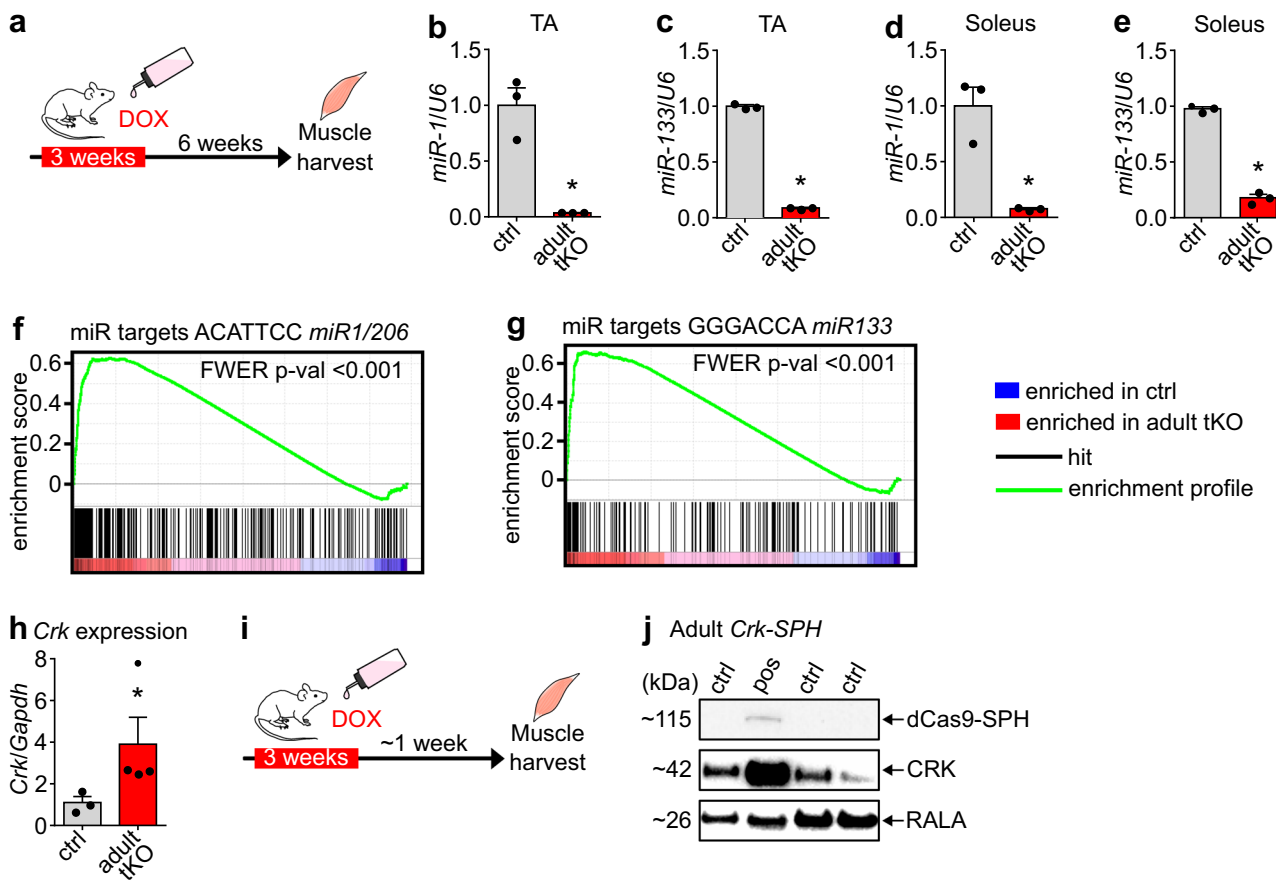


Fig. 6 Loss of *miR-1/206/133* in adult mice increases CRK levels. **a-e** Deletion of *miR-1/133* in adult muscle was induced by doxycycline (DOX) application in *miR-1-1/133a-2^{-/-}//miR-1-2/133a-1^{lox/lox}//miR-206/133b^{-/-}//HSA-rtTA-TRE-Cre^{+/-}* mice (**a**). Doxycycline treatment strongly reduced expression of *miR-1* (**b, d**) and *miR-133a* (**c, e**) in TA (**b, c**) and soleus (**d, e**) muscles of control and adult *miR-1/206/133* tKO mice tested via TaqMan assays ($n = 3$ control/3 tKO, control = *miR-1-1/133a-2^{+/+}//miR-1-2/133a-1^{lox/lox}//miR-206/133b^{+/+}//HSA-rtTA-TRE-Cre^{+/+}*, Mann-Whitney-U test, one-tailed, $*p = 0.05$ [male, 15-17 weeks old]). *U6 snRNA* served as control. **f, g** GSEA of adult *miR-1/206/133* tKO ($n = 3$) and control ($n = 2$) TA muscles reveals enrichment of predicted *miR-1/206* and *miR-133* targets in adult tKO (control = *miR-1-1/133a-2^{-/-}//miR-1-2/133a-1^{lox/lox}//miR-206/133b^{-/-}//HSA-rtTA-TRE-Cre^{+/+}*, familywise-error rate method (FWER), $p < 0.001$ (**f, g**) [male, -44 weeks]). **h** Adult *miR-1/206/133* tKO ($n = 4$) show elevated *Crk* expression tested via TaqMan assay in TA muscles ($n = 3$, control = *miR-1-1/133a-2^{-/-}//miR-1-2/133a-1^{lox/lox}//miR-206/133b^{-/-}//HSA-rtTA-TRE-Cre^{+/+}*, Mann-Whitney-U test, one-tailed, $*p = 0.0286$ [male, female, -44 weeks]). *Gapdh* served as control. **i, j** Western blot analysis shows HSA-rtTA-TRE-Cre dependent dCas9-SPH expression and elevated CRK expression in quadriceps muscle of adult *sgRNA^{+/-}//HSA-rtTA-TRE-Cre^{+/-}//CAG-LSL-dCas9-SPH^{+/-}* mice ($n = 1$ adult *Crk-SPH*) ($n = 3$, control = littermates *HSA-rtTA-TRE-Cre^{+/+}* or *CAG-LSL-dCas9-SPH^{+/+}*, [male, female; 21 weeks]). RALA served as loading control. Source data are provided as a Source Data file. Data are presented as mean values \pm SEM in **b-e** and **h**.

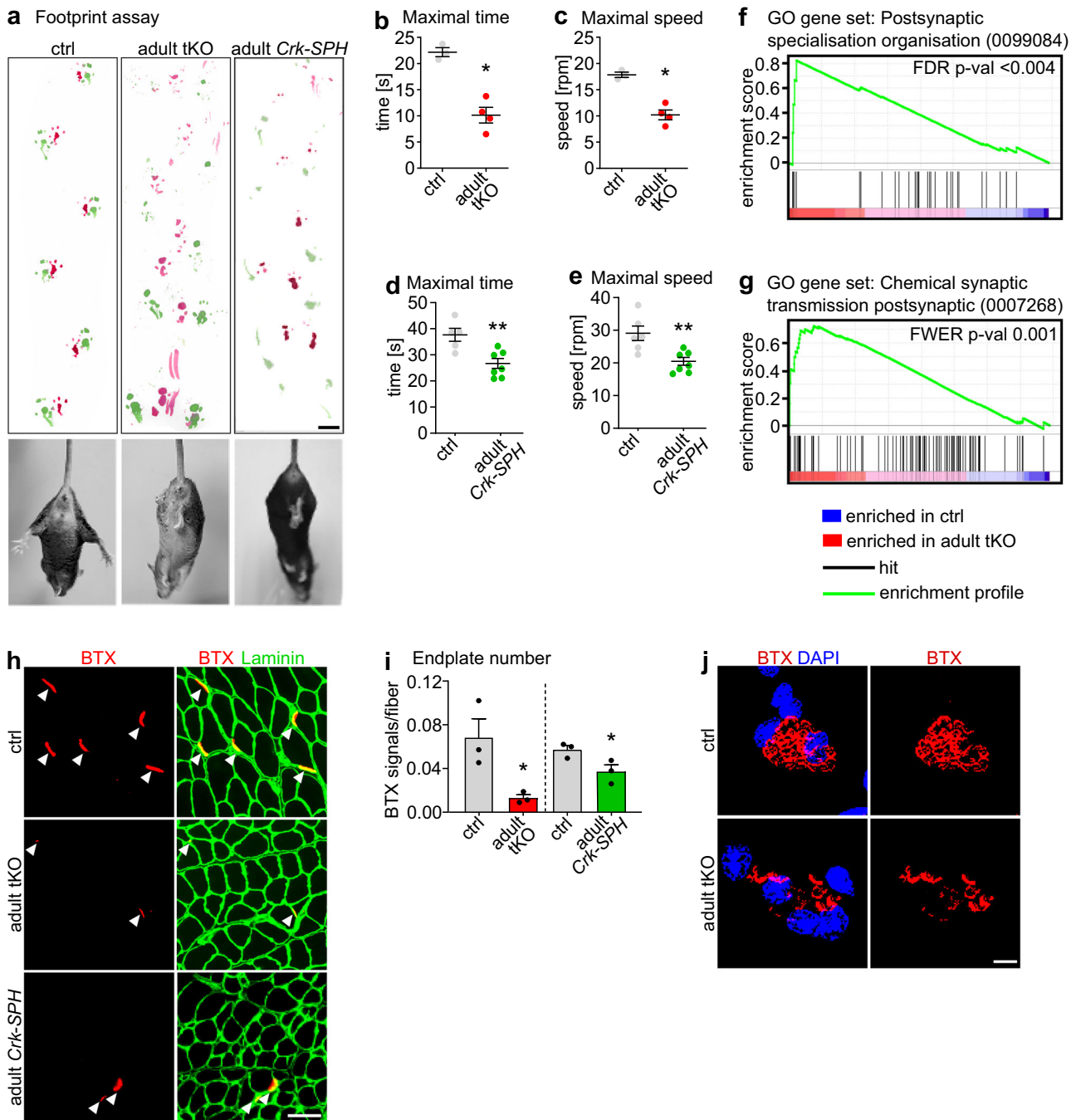


Fig. 7 Maintenance of NMJ in adult mice requires *miR-1/206/133*-dependent regulation of CRK. **a** Adult *miR-1/206/133* tKO ($n = 4$) and adult *Crk-SPH* ($n = 3$) show muscle weakness, abnormal locomotion in footprint assays, and hindlimb clasping during tail suspension ($n = 3$, control = *miR-1-1/133a-2^{-/-}/miR-1-2/133a-1^{lox/lox}/miR-206/133b^{-/-}/HSA-rtTA-TRE-Cre^{+/+}* [control and tKO female -44 weeks; adult *Crk-SPH* 13-16 weeks, females]). Scale-bar: 1 cm. **b, c** Adult *miR-1/206/133* tKO ($n = 4$) show impaired motor function in Rotarod tests ($n = 3$, control = *miR-1-1/133a-2^{-/-}/miR-1-2/133a-1^{lox/lox}/miR-206/133b^{-/-}/HSA-rtTA-TRE-Cre^{+/+}* [male, female, ~44 weeks]; Mann-Whitney-U test, one-tailed, $*p = 0.0286$). **d-e** Adult *Crk-SPH* mice show impaired motor functions in Rotarod tests ($n = 6$, control = *CAG-LSL-dCas9-SPH^{+/+}*, $n = 7$ *Crk-SPH* animals [female, 13-16 weeks]; Mann-Whitney-U test, one-tailed, $**p = 0.0051$ (**d**), $**p = 0.0029$ (**e**)). **f, g** GSEA of adult *miR-1/206/133* tKO ($n = 3$) and control ($n = 2$) TA (control = *miR-1-1/133a-2^{-/-}/miR-1-2/133a-1^{lox/lox}/miR-206/133b^{-/-}/HSA-rtTA-TRE-Cre^{+/+}*, familywise-error rate method (FWER), $p = < 0.004$ (**f**), false discovery rate (FDR) $p = 0.001$ (**g**) [male, -44 weeks]). **h, i** Quantification of BTX-stained postsynaptic regions in TA transversal sections from adult *miR-1/206/133* tKO ($n = 3$) and adult *Crk-SPH* ($n = 3$) mice in comparison to controls ($n = 3$, control of adult tKO = *miR-1-1/133a-2^{-/-}/miR-1-2/133a-1^{lox/lox}/miR-206/133b^{-/-}/HSA-rtTA-TRE-Cre^{+/+}*, [-44 weeks, male]; $n = 3$, control of *Crk-SPH* = *HSA-rtTA-TRE-Cre^{+/+}* or *CAG-LSL-dCas9-SPH^{+/+}* [10-14 weeks, female], Mann-Whitney-U tests, one tailed, $*p = 0.05$). Scale-bar in **r**: 50 μm . **j** BTX staining (red) of isolated single myofibers of *flexor digitorum brevis* muscle from adult *miR-1/206/133* tKO ($n = 3$) in comparison to controls ($n = 3$, control of adult *miR-1/206/133* tKO = *miR-1-1/133a-2^{-/-}/miR-1-2/133a-1^{lox/lox}/miR-206/133b^{-/-}/HSA-rtTA-TRE-Cre^{+/+}*, [-44 weeks, male]). DAPI staining in blue. Z-stacks. Scale-bar: 20 μm . Source data are provided as a Source Data file. Data are presented as mean values \pm SEM in **b-e** and **i**.

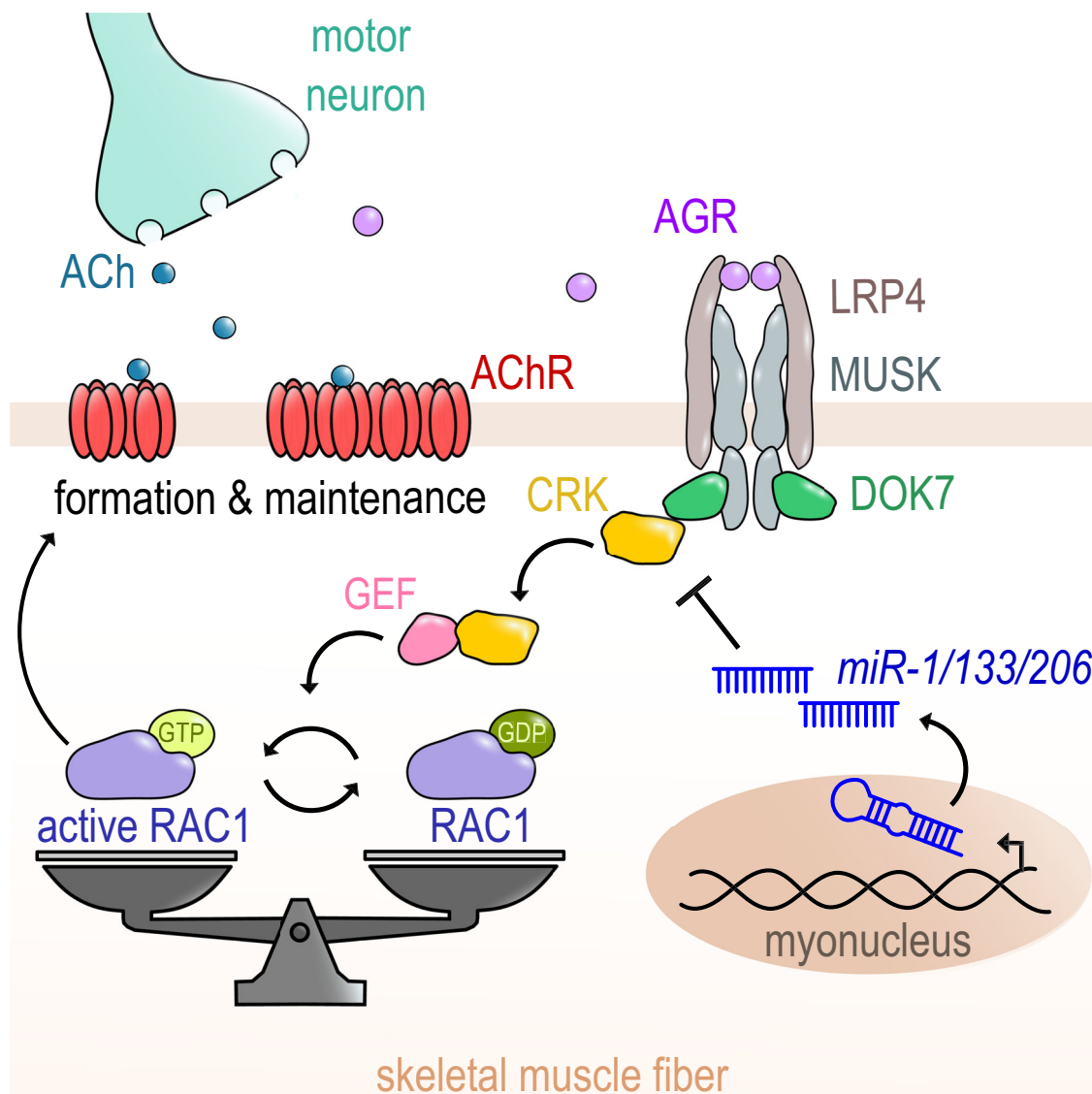


Fig. 8 Regulation of CRK-RAC1 activity by the *miR-1/206/133* miRNA family is essential for neuromuscular junction function. The muscle-specific miRNAs of the *miR-1/206/133* family are crucial regulators of a postsynaptic signaling cascade comprising DOK7-CRK-RAC1, critical for stabilization and anchoring of AChRs during NMJ development and maintenance. ACh (Acetylcholine), AChR (Acetylcholine receptor), AGR (Agrin), CRK (Adapter protein CRK), DOK7 (Docking Protein 7), GDP (Guanosine diphosphate), GEF (Guanine nucleotide exchange factor), GTP (Guanosine triphosphate), LRP4 (Low-density lipoprotein receptor-related protein 4), MuSK (Muscle-specific kinase), RAC1 (Rac family small GTPase 1).

(synaptic cell adhesion molecule) to promote postsynaptic cytoskeletal dynamics³¹. We demonstrated that enhanced RAC1 activation due to increased CRK expression prevents formation of proper AChR-macro-clusters. Interestingly, tight control of CRK levels is also important to maintain distribution, number, and functionality of NMJs in adult mice. We observed a striking neuromuscular phenotype already one week after completing the 3-weeks DOX treatment to initiate *Crk* overexpression, which argues for an active role of CRK in securing integrity of the NMJ structure. We cannot completely rule out that the increased *Crk* expression interferes with turnover of individual components of the NMJ-complex, but NMJs have been described as relatively stable structures⁴⁶, making it unlikely that disturbed turnover is responsible for the rapid onset of the neuromuscular phenotype in adult *Crk-SPH* animals. The late onset of the neuromuscular phenotype in adult *miR-1/206/133* tKO mice is most likely due to slow clearance of highly expressed *miR-1/206/133* miRNAs,

which has been noticed before^{14,47}. The rather long time required for downregulation of *miR-1/206/133* miRNA concentrations suggests that these miRNAs are essential to establish long-lasting cellular functions but are not involved in acute regulatory processes.

Adult *miR-1/133a* dKO mice are characterized by upregulation of *Dlk-Dio3* miRNA/lncRNA mega-cluster and mitochondrial dysfunctions¹⁴, a phenotype that was absent in neonatal but not in adult *miR-1/206/133* tKO skeletal muscles. The stage-specific functions of *miR-1/206/133* indicate that miRNAs serve different roles that strongly depend on specific cellular requirements. The same principle was observed for the role of *miR-1/133a* during embryonic heart development, where *miR-1/133a* primarily regulate the switch from primitive smooth muscle gene expressing to more differentiated cardiomyocytes by repressing myocardin and other smooth muscle-specific genes¹². Another surprising feature of the *miR-1/206/133* family, given the high expression of

individual genes of this family, are concentration-dependent specific functions that manifest as partial redundancy. Adult *miR-1/133a* dKO mice display a mitochondrial but not an NMJ phenotype, whereas adult *miR-1/206/133* tKO animals show both a mitochondrial as well as an NMJ phenotype, although the seed sequences of *miR-1* and *miR-206* or *miR-133a* and *miR-133b* are identical. Absence of a single *miR-206/133b* or *miR-1/133a* miRNA cluster of the *miR-1/206/133* family does not disturb development of the neuromuscular endplate. After loss of two *miR-1/133a* cluster (dKO), the remaining *miR-206/133b* cluster is upregulated, which compensates for the absence of the other clusters in both neonates and adults, enabling normal NMJ development and maintenance. Similarly, inactivation of a single heart-specific *miR-1/133a* cluster is not sufficient to prevent the switch from primitive smooth muscle gene expressing to more differentiated cardiomyocytes⁴⁸. These findings suggest that absolute concentrations of individual miRNAs participate in determining target specificity, probably due the relative efficiency of miRNA-mediated repression for each specific target. Moreover, efficiency of repression may also depend on expression levels of miRNA targets, presence of RNA-binding proteins masking miRNA target sites, regulation of posttranscriptional processing of miRNAs, and RNA-modifications^{47,49,50}.

The abundance of *miR-1/206/133* and/or their targets may change under disease conditions and exaggerate the role of individual miRNAs of the *miR-1/206/133* family. In a previous study, it was reported that deficiency of *miR-206* alone is sufficient to accelerate progression of ALS⁵¹. In the same report, it was also claimed that *miR-206* is required for efficient regeneration of neuromuscular synapses, although in a later report from the same group no innervation defects were observed after inactivation of *miR-206* in mdx mice, a commonly used model for muscle regeneration⁵². In contrast, formation of neuromuscular synapses was not affected in *miR-206* mutants⁵¹, which is in line with our results. We assume that expression of *Crk* or other *miR-1/206/133* targets may change under certain disease conditions, which might make the *miR-1/206/133*-CRK-FARP1-RAC1 axis more vulnerable to even small changes in the concentration of *miR-1/206/133* as in *miR-206* knock-out mice.

The stage- and concentration-dependent functions of *miR-1/206/133* create an impressive specificity that allows regulation of a wide range of different developmental and physiological processes according to cellular needs. The regulation of *Crk* represents a paradigmatic example for this principle. CRK is a universal adapter molecule, requiring differential stage-specific regulatory input in different cell types. In myofibers, *miR-1/206/133* have evolved to serve this function and adjust CRK concentrations to support NMJ formation and maintenance. In contrast, cardiomyocytes do not own NMJs and therefore do not require the combined activity of *miR-1/206/133* to regulate *Crk*. It was surprising to learn that *miR-1/206/133* in skeletal muscles are not involved in lineage specification, development, and differentiation as in the heart but primarily direct specific physiological processes. Similarly, *miR-1/206/133* do not play a decisive function in the regulation of MuSCs, which is at odds with previous publications (reviewed in ref. ⁵³). In this context, it is important to point out that our data rely on clean genetic models avoiding potential off-targets effects that are inevitably associated with the use of antagomirs, GAPmers or other similar techniques^{54–56}. On the other hand, germline inactivation of genes may initiate compensatory mechanisms that can disguise specific functions of deleted genes, which may account for differences between miRNA-silencing by antagomirs and genetic approaches. However, we also inactivated *miR-1/206/133* in MuSC and myofibers using inducible Cre-recombinases, essentially eliminating long-term adaptive compensations.

The *miR-1/206/133* target sites in *Crk* are conserved between mice and humans, suggesting that posttranscriptional repression of CRK by *miR-1/206/133* is also operative in other mammalian species. Interestingly, mutations of *Dok7* have been described in human individuals with CMS⁶. The most common mutations of *Dok7* result in C-terminal truncations of DOK7, which may prevent recruitment of CRK and CRK-L, thereby causing NMJ synaptopathy⁴. It seems likely that mutations or processes, which increase the level of CRK account for some cases of idiopathic CMS in humans. Taken together, our findings provide insights into the pathogenesis of human neuromuscular diseases and demonstrate the enormous complexity of regulatory interactions exerted by *miR-1/206/133*.

Methods

Study approval. All animal experiments were done in accordance with the Guide for the Care and Use of Laboratory Animals published by the US National Institutes of Health (NIH Publication No. 85-23, revised 1996) and were approved by the responsible Committee for Animal Rights Protection of the State of Hessen (Regierungspraesidium Darmstadt, Wilhelmstr. 1-3, 64283 Darmstadt, Germany) with the project number B2-1054 and B2-1234.

Animal models. Germline deletion of *miR-1/206/133* (ctKO) was achieved by combining deletion alleles of *miR-1/133a* clusters on mouse chromosome 2 and 18¹² to loss of function alleles of the *miR-206/133b* miRNA cluster¹⁷. Muscle-specific deletion of the *miR-1/206/133* miRNAs (tKO) was achieved using *Pax7-Cre* mice²¹ in combination with *miR-1-1/miR-133a-2^{-/-}/miR-1-2/miR-133a-1^{lox/lox}*¹⁴ and *miR-206/133b^{-/-}* alleles¹⁷. *miR-1/206/133* were specifically deleted in adult MuSCs (muscle stem cells) by combination of conditional miRNA cluster alleles with *Pax7-CreERT2*⁵⁷. Activation of Cre recombinase activity in adult MuSC was induced by tamoxifen injection (i.p. 75 mg/kg BW/day for 5 days at 8–10 weeks of age). Deletion of *miR-1/206/133* specifically in adult myofibers was achieved using the *HSA-rtTA/TRE-Cre* mouse line³⁶. Recombination efficiency in adult myofibers was confirmed by mating of *HSA-rtTA/TRE-Cre* mice to the *Z/AP* reporter strain³⁷. Recombination of *Z/AP* or miRNA deletion in adult myofibers was induced by administration of 2 mg/ml doxycycline (Sigma #D9891) with 5% sucrose (Roth #9097.1) in drinking water ad libitum for 3 weeks.

For forced skeletal muscle-specific expression of *Crk*, the ORF of *Crk* was amplified using a DNAbank Fantom2Clone (AK028488, ENSMUST00000017920.13) and oligonucleotides atcgggactctgATTTCGGGCGTGTCTGGGAGGCTG and cgactgacccCATCTCTGTCAGCAAAGTGTGAGC. BamHI digested PCR-fragment was inserted into the pSG5-HSA-MCM vector (kind gift from Karyn Esser;³²) after deletion of the MCM by EcoRI digestion, relegation and subsequent BamHI digestion. The resulting pSG5-HSA-CRK vector was digested using DrrI and PvuI and the resulting HSA-CRK expression cassette was used for pronuclear injection to generate transgenic mice. Transgenic mice were recovered at E18.5 and presence of the transgene was determined by PCR using transgene-specific oligonucleotides (CCCAGCCGAG AGTAGCAGTTGTAG, CATCTTCCCAITCTAAACAACACCC).

CRISPR-dCas9-activator-dependent overexpression of *Crk* in skeletal muscle transgenic mice was achieved using specific sgRNA that recruits the dCas9-SPH complex (CAG-LSL-dCas9-SunTag-p65-HSF1) to the *Crk* promoter after activation of dCas9-SPH complex expression by *Pax7-Cre* or *HSA-rtTA/TRE-Cre*³³. Different predicted highly effective sgRNA sequences³⁴ were used to amplify expression cassettes consisting of U6 promoter, sgRNA and termination sequence using PCR strategy⁵⁸. (sgRNA oligonucleotide #A GTGGAAAGGACGAAAC ACCGGGCCAACCGCGGAGGATGGGGGTTTTAGAGCTAGAAATAG; #B GTGGAAAGGACGAAACACCGGGAGTGCATGCGGCCTCTGTTTTAG AGCTAGAAATAG; #C GTGGAAAGGACGAAACACCGGGGACGCCCCGCC ATTGGGAGAGTTTTAGAGCTAGAAATAG; #D GTGGAAAGGACGAAAC ACCGGGAGCGGAGTCTAGGTCTAAGTTTTAGAGCTAGAAATAG; #E GTGGAAAGGACGAAACACCGGGGACCCCAACCGCGGAGGATGTTTTAG AGCTAGAAATAG). Each generated sgRNA was combined with a U6 promoter derived from plasmid pX459 using PCR. pSpCas9(BB)-2A-Puro (pX459) V2.0 was a gift from Feng Zhang (Addgene plasmid #62988; <http://n2t.net/addgene:62988>; RRID: Addgene_62988)⁵⁹. Individual expression cassettes were tested for activation of *Crk* transcription in C2 cells in combination with the Sp-dCas9-VPR system. Sp-dCas9-VPR was a gift from George Church (Addgene plasmid #63798; <http://n2t.net/addgene:63798>; RRID: Addgene_63798)³⁵. Co-transfections were performed using Lipofectamine 3000 (ThermoFisher #L3000075) according to the manufacturer's protocol. The most effective sgRNA cassette (*Crk*-sgRNA #C) was used for pronuclear injection to generate transgenic mice, which used to generate *sgRNA^{+/-}/Pax7-Cre^{+/-}/CAG-LSL-dCas9-SunTag-p65-HSF1^{+/-}* (*Crk*-SPH) and *sgRNA^{+/-}/HSA-rtTA/TRE-Cre^{+/-}/CAG-LSL-dCas9-SunTag-p65-HSF1^{+/-}* (adult *Crk*-SPH) mice. Presence of the sgRNA was confirmed by PCR (GTAAACACGACGCGCCAG TGAGGGCCTATTTCCCATGATTC, AGGAAACAGCTATGACCATGAAAAA AAGCACCGACTCGGTGCCAC). (*Pax7-Cre*: GGATAGTGAAACAGGGGCAA, GCTCTGGATACACCTGAGTCT, TCGGCTTCTTCTAGGTTCTGCTC; CAG-

(3 × 5 min) and two washing steps with PBS. Next, myotubes were incubated with blocking solution for 1 h at 37 °C in a humid chamber. The PLA was done using a combination of two different primary antibodies (anti-CRK Santa Cruz #sc-390132; anti-FARP1 ThermoFisher #PA5-99105), produced either in rabbit or mouse. Antibodies were applied to cells at a dilution of 1:1000 and incubated overnight at 4 °C. Following PLA probe incubation, ligation and signal amplification, a Wheat germ agglutinin (WGA) Alexa Fluor 488 Conjugate (ThermoFisher #W11261) staining was performed at a dilution of 1:300 in PBS for 20 min.

miRNA target prediction analysis. Potential microRNA target mRNAs were identified using the miRNA target prediction database [microrna.org](http://www.microrna.org) version 2010 (<http://www.microrna.org>).

Whole-mount in situ hybridization. Whole-mount in situ hybridization was performed as described⁶². Briefly, the antisense probe was generated from a plasmid containing a Myogenin cDNA (Source Bioscience clone #IMAGp998A011039Q) with polyA removed by NotI/HpaI digestion and re-ligation using the XhoI linearized plasmid template in combination with DIG-RNA labelling Mix (Roche #11277073910) and T3 RNA polymerase (Promega #P2083). Unincorporated nucleotides were removed by precipitation of the probe. Embryos of the indicated stage were isolated, fixed using 4% PFA/PBS for 2 h and transferred using PBT (0.1% Tween20/PBS; 2 × 5 min), 25% methanol/PBT, 50% methanol/PBT, 75% methanol/PBT (5 min each step) to methanol (−20 °C, overnight). Samples were processed using 75% methanol/PBT, 50% methanol/PBT, 25% methanol/PBT, 2 × PBT (5 min each) to 6% H₂O₂/PBT (1 h, Sigma #H1009). Samples were washed using PBT (3 × 5 min), incubated in 10 µg/ml Proteinase K/PBT (10 min, 21 °C), 2 mg/ml glycine/PBT (5 min), washed using PBT (2 × 5 min) and incubated in hybridization solution (50% Formamide, 5 × SSC pH 4.5, 1% SDS, 50 µg/ml yeast tRNA, 50 µg/ml heparin) at 70 °C. After 1 h of prehybridization, probe was added (0.1 µg/ml f. c.) and hybridization was performed overnight at 70 °C. Embryos were transferred to 50% formamide, 5 × SSC pH 4.5, 1% SDS (2 × 30 min, 70 °C), 10 mM Tris HCl pH 7.5, 0.5 M NaCl, 0.1% Tween 20 (2 × 5 min, room temperature), 50% formamide, 2 × SSC pH 4.5 (2 × 30 min, 65 °C), MAB solution (3 × 5 min; 100 mM malic acid pH 7.5, 150 mM NaCl), blocking solution (1 h; MAB, 2% blocking reagent [Roche #11096176001], 20% FCS), to anti-Digoxigenin-AP Fab fragments (1:2000, Roche #11093274910 in blocking solution, overnight). Samples were washed using MAB (3 × 5 min, 4 × 1 h), NTMT (3 × 10 min, 100 mM TrisHCl pH 9.5, 50 mM MgCl₂, 1% Tween-20; 2 mM Levamisole) and stained in staining solution (21 °C, NBT/BCIP Roche #11681451001 1:50 in NTMT). After staining, embryos were washed in PBT (3 × 5 min) and stored in 50% Glycerol/PBT. All incubations were done at 4 °C unless indicated otherwise.

Transcriptome analysis and TaqMan assays. RNA obtained from tissue and cells were isolated using peqGOLD TriFast (VWR #30-2010DE) according to the manufacturer's instructions. RNA was isolated from E18.5 quadriceps muscles and from TA and soleus muscles of adult 12–44 weeks old mice (number of animals are indicated in figure legends). RNA labelling and hybridization to Affymetrix MTA1-0 arrays followed the manufacturer's instructions. Data were analyzed using ArrayStar12 with RMA and evaluated using Student's t-test. Gene set enrichment analysis (GSEA)⁶³ was performed using GSEA Java desktop software application v3.0 with default parameters using the permutation type gene set. GSEA determines whether a predefined set of genes shows statistically significant, concordant differences between two biological states and thus helps to identify relevant biological processes⁶³. Expression of mature miRNAs and of other transcripts was quantified using FAM labelled TaqMan Gene Expression Assays (ThermoFisher *Crk* #Mm00467065_m1) or TaqMan MicroRNA Assays (ThermoFisher: *miR-1* #002222, *miR-133a* #002246, *miR-206* #000510), respectively. The microRNA Reverse Transcription Kit (#4366596) was used to convert miRNA into cDNA. The TaKaRa Kit (#RR047A) was used for cDNA synthesis of other transcripts. *U6 snRNA* (ThermoFischer #001973) and *Gapdh* (ThermoFischer #Mm999999915) were used as controls. Relative expression was calculated using the $\Delta\Delta C_t$ method (StepOne Software v2.3).

Western blot analysis and immunofluorescence staining. Western blots and immunofluorescence staining were done following established procedure. An extended description is provided in the Supplementary Information file. Skeletal muscle was lysed by sonication. The protein extracts were separated on a SDS-PAGE and blotted onto nitrocellulose membranes. After the blocking of membranes primary antibodies were used to probe the blots overnight. The secondary antibodies were incubated for 1 h. Quantification of western blots was performed by densitometric scanning.

Cultured cells, isolated myofibers and cryosections were mounted on Superfrost slides and used for immunofluorescence staining. Samples were fixed and washed. Blocking was performed for 1 h. Afterwards the sections were incubated with primary antibodies overnight at 4 °C. Subsequently, the sections were washed and incubated with secondary antibodies and BTX, followed by washing steps. The samples were embedded using Fluoromount W. The Image J software 1.53k was employed for measuring the size of cross-sectional area of Laminin-stained fibers.

Whole-mount staining of the diaphragm followed published protocols⁶⁴. Diaphragm muscles were isolated and stained with α -Bungarotoxin and with antibodies against SV2 and neurofilament. Afterwards, samples were flat-mounted and embedded. The width of AChR endplate zone measured using ImageJ. The AChR cluster size and number was quantified either from serial TA and paraspinal muscle transversal sections or from whole mount diaphragm Z-stack data.

Pull down assays of active RAC1. To monitor RAC1 activity after transient overexpression of CRK (pIRESII-EGFP-CRK vector) in C2 cells the Active RAC1 Pull-Down and Detection Kit (ThermoFisher #16118) was used according to the manufacturer's protocol. The kit is based on a GST-fusion protein containing the PBD (p21-binding domain) of PAK1 (human p21-activated protein kinase 1) and glutathione agarose resin to specifically pull down active RAC1. A specific anti-RAC1 antibody was used for detection of RAC1-GTP and total RAC1 on western blot. The western blot procedure was performed as described above. Pull-down assay were performed with samples from three independent transfections per experiment and three independent pull down assays. For analysis, the ratios of RAC1-GTP to total RAC1 were calculated.

Mass spectrometry (MS). MS was done following established procedure. An extended description is provided in the Supplementary Information file. Triplicate samples of E18.5 mouse quadriceps were lysed for whole skeletal muscle proteomics. After determining the concentration of the resulting peptide mixture, equal amounts of peptides were subjected to stable isotope labeling using reductive dimethylation^{65,66}. Labeling efficiency was confirmed to be >95% by LC/MS2 and differentially labeled samples mixed 1:1, followed by subsequent desalting using oligo R3 columns. For greater sequencing depth, samples were separated into eight fractions, followed by final desalting, concentration and storage on STAGE tips⁶⁷.

Triplicate sample sets of affinity purified CRK from wild type, as well as *miR-1/206/133* tKO E18.5 limb muscle samples were subjected to in gel digest to detect interaction partners of CRK⁶⁸. Processed samples were analyzed using liquid chromatography/tandem-mass spectrometry (LC/MS2). Relevant instrumentation parameters are included in the supplementary information (Supplementary Data 1)⁶⁹. Peptide/spectrum matching, as well as quantitation was performed using the MaxQuant suite of algorithms (proteome: v. 1.6.0.1; interactome: v. 1.6.6.0^{70–72}); against the canonical and isoforms UniProt mouse database (proteome: downloaded 2017/04/20, 97484 entries; interactome: downloaded 2019/08/19, 86161 entries⁷³); using parameters documented in the supplementary material (Supplementary Data 1). Downstream bioinformatics analysis was performed using a limma-based R pipeline⁷⁴ (<https://github.com/bhagwataditya/autonomics>).

Statistics and quantification. Statistical analysis was performed using GraphPad Prism 6.07. Data are depicted as mean ± SEM. Data values were tested for Gaussian distribution. Student's t-test was used as indicated in the figure legends when distribution of data normal. Non-parametric statistical tests were used as indicated, when normality of data distribution could not be confirmed.

Reporting summary. Further information on research design is available in the Nature Research Reporting Summary linked to this article.

Data availability

Data have been deposited in public data bases. Microarray data are available at Arrayexpress (E-MTAB-10229; E-MTAB-10228; E-MTAB-10227). Proteome data are available at ProteomeCentral [<http://proteomecentral.proteomexchange.org/cgi/GetDataset?ID=PX032882>] with the dataset identifier (JPST001553) PXD032882. Source data are provided as a Source Data file.

Received: 3 June 2021; Accepted: 7 May 2022;

Published online: 08 June 2022

References

- Li, L., Xiong, W. C. & Mei, L. Neuromuscular junction formation, aging, and disorders. *Annu. Rev. Physiol.* **80**, 159–188 (2018).
- Herbst, R. MuSk function during health and disease. *Neurosci. Lett.* **716**, 134676 (2020).
- Belotti, E. & Schaeffer, L. Regulation of Gene expression at the neuromuscular Junction. *Neurosci. Lett.* **735**, 135163 (2020).
- Hallock, P. T. et al. Dok-7 regulates neuromuscular synapse formation by recruiting Crk and Crk-L. *Genes Dev.* **24**, 2451–2461 (2010).

5. Bergamin, E., Hallock, P. T., Burden, S. J. & Hubbard, S. R. The cytoplasmic adaptor protein Dok7 activates the receptor tyrosine kinase MuSK via dimerization. *Mol. Cell* **39**, 100–109 (2010).
6. Beeson, D. et al. Dok-7 mutations underlie a neuromuscular junction synaptopathy. *Science* **313**, 1975–1978 (2006).
7. Hamuro, J. et al. Mutations causing DOK7 congenital myasthenia ablate functional motifs in Dok-7. *J. Biol. Chem.* **283**, 5518–5524 (2008).
8. Burden, S. J., Huijbers, M. G. & Remedio, L. Fundamental molecules and mechanisms for forming and maintaining neuromuscular synapses. *Int. J. Mol. Sci.* **19**, 490 (2018).
9. Bai, Y. et al. Balanced Rac1 activity controls formation and maintenance of neuromuscular acetylcholine receptor clusters. *J. Cell Sci.* **131**, jcs215251 (2018).
10. Boettger, T. & Braun, T. A new level of complexity: The role of microRNAs in cardiovascular development. *Circ. Res.* **110**, 1000–1013 (2012).
11. Coenen-Stass, A. M. et al. Selective release of muscle-specific, extracellular microRNAs during myogenic differentiation. *Hum. Mol. Genet* **25**, 3960–3974 (2016).
12. Wystub, K., Besser, J., Bachmann, A., Boettger, T. & Braun, T. miR-1/133a clusters cooperatively specify the cardiomyogenic lineage by adjustment of myocardin levels during embryonic heart development. *PLoS Genet.* **9**, e1003793 (2013).
13. Heidersbach, A. et al. microRNA-1 regulates sarcomere formation and suppresses smooth muscle gene expression in the mammalian heart. *Elife* **2**, e01323 (2013).
14. Wust, S. et al. Metabolic maturation during muscle stem cell differentiation is achieved by miR-1/133a-mediated inhibition of the Dlk1-Dio3 mega gene cluster. *Cell Metab.* **27**, 1026–1039 e1026 (2018).
15. Valussi, M. et al. Repression of Osmr and Fgfr1 by miR-1/133a prevents cardiomyocyte dedifferentiation and cell cycle entry in the adult heart. *Sci. Adv.* **7**, eabi6648 (2021).
16. Liu, N. et al. microRNA-133a regulates cardiomyocyte proliferation and suppresses smooth muscle gene expression in the heart. *Genes Dev.* **22**, 3242–3254 (2008).
17. Boettger, T., Wust, S., Nolte, H. & Braun, T. The miR-206/133b cluster is dispensable for development, survival and regeneration of skeletal muscle. *Skelet. Muscle* **4**, 23 (2014).
18. Mitchelson, K. R. & Qin, W. Y. Roles of the canonical myomiRs miR-1, -133 and -206 in cell development and disease. *World J. Biol. Chem.* **6**, 162–208 (2015).
19. Koutsoulidou, A., Mastroiannopoulos, N. P., Furling, D., Uney, J. B. & Phylactou, L. A. Expression of miR-1, miR-133a, miR-133b and miR-206 increases during development of human skeletal muscle. *BMC Developmental Biol.* **11**, 34 (2011).
20. Lewis, B. P., Shih, I. H., Jones-Rhoades, M. W., Bartel, D. P. & Burge, C. B. Prediction of mammalian microRNA targets. *Cell* **115**, 787–798 (2003).
21. Keller, C., Hansen, M. S., Coffin, C. M. & Capecchi, M. R. Pax3:Fkhr interferes with embryonic Pax3 and Pax7 function: Implications for alveolar rhabdomyosarcoma cell of origin. *Genes Dev.* **18**, 2608–2613 (2004).
22. Simpson, B., Rich, M. M., Voss, A. A. & Talmadge, R. J. Acetylcholine receptor subunit expression in Huntington's disease mouse muscle. *Biochem Biophys. Rep.* **28**, 101182 (2021).
23. Ferraro, E., Molinari, F. & Berghella, L. Molecular control of neuromuscular junction development. *J. Cachexia Sarcopenia Muscle* **3**, 13–23 (2012).
24. Cheerathodi, M. & Ballif, B. A. Identification of CrkL-SH3 binding proteins from embryonic murine brain: Implications for Reelin signaling during brain development. *J. Proteome Res* **10**, 4453–4462 (2011).
25. Birge, R. B., Kalodimos, C., Inagaki, F. & Tanaka, S. Crk and CrkL adaptor proteins: networks for physiological and pathological signaling. *Cell Commun. Signal* **7**, 13 (2009).
26. Feller, S. M. Crk family adaptors-signalling complex formation and biological roles. *Oncogene* **20**, 6348–6371 (2001).
27. Rao, P. K., Kumar, R. M., Farkhondeh, N., Baskerville, S. & Lodish, L. F. Myogenic factors that regulate expression of muscle-specific microRNAs. *PNAS* **23**, 8721–8726 (2006).
28. Yeo, M. G. & Song, W. K. v-Crk regulates membrane dynamics and Rac activation. *Cell Adh Migr.* **2**, 174–176 (2008).
29. Weston, C., Yee, B., Hod, E. & Prives, J. Agrin-induced Acetylcholine receptor clustering is mediated by the small guanosine triphosphatases Rac and Cdc42. *J. Cell Biol.* **150**, 205–212 (2000).
30. Weston, C. et al. Cooperative regulation by Rac and Rho of agrin-induced acetylcholine receptor clustering in muscle cells. *J. Biol. Chem.* **278**, 6450–6455 (2003).
31. Cheadle, L. & Biederer, T. The novel synaptogenic protein Farp1 links postsynaptic cytoskeletal dynamics and transsynaptic organization. *J. Cell Biol.* **199**, 985–1001 (2012).
32. McCarthy, J. J., Srikuea, R., Kirby, T. J., Peterson, C. A. & Esser, K. A. Inducible Cre transgenic mouse strain for skeletal muscle-specific gene targeting. *Skelet. Muscle* **2**, 8 (2012).
33. Zhou, H. et al. In vivo simultaneous transcriptional activation of multiple genes in the brain using CRISPR-dCas9-activator transgenic mice. *Nat. Neurosci.* **21**, 440–446 (2018).
34. Horlbeck, M. A. et al. Compact and highly active next-generation libraries for CRISPR-mediated gene repression and activation. *Elife* **5**, e19760 (2016).
35. Chavez, A. et al. Highly efficient Cas9-mediated transcriptional programming. *Nat. Methods* **12**, 326–328 (2015).
36. Rao, P. & Monks, D. A. A tetracycline-inducible and skeletal muscle-specific Cre recombinase transgenic mouse. *Dev. Neurobiol.* **69**, 401–406 (2009).
37. Lobe, C. G. et al. Z/AP, a double reporter for Cre-mediated recombination. *Developmental Biol.* **208**, 281–292 (1999).
38. Brooks, S. P. & Dunnett, S. B. Tests to assess motor phenotype in mice: a user's guide. *Nat. Rev. Neurosci.* **10**, 519–529 (2009).
39. Guy, J., Hendrich, B., Holmes, M., Martin, J. E. & Bird, A. A mouse Mecp2-null mutation causes neurological symptoms that mimic Rett syndrome. *Nat. Genet.* **27**, 322–326 (2001).
40. Hayward, L. J. et al. Targeted mutation of mouse skeletal muscle sodium channel produces myotonia and potassium-sensitive weakness. *J. Clin. Invest* **118**, 1437–1449 (2008).
41. Eguchi, T., Tezuka, T., Miyoshi, S. & Yamanashi, Y. Postnatal knockdown of dok-7 gene expression in mice causes structural defects in neuromuscular synapses and myasthenic pathology. *Genes Cells* **21**, 670–676 (2016).
42. Park, T. J., Boyd, K. & Curran, T. Cardiovascular and craniofacial defects in Crk-null mice. *Mol. Cell Biol.* **26**, 6272–6282 (2006).
43. Huang, Y. et al. CRK proteins selectively regulate T cell migration into inflamed tissues. *J. Clin. Invest* **125**, 1019–1032 (2015).
44. Bhatt, V. S., Zeng, D., Krieger, I., Sacchetti, J. C. & Cho, J. H. Binding mechanism of the N-Terminal SH3 Domain of CrkII and Proline-Rich Motifs in cAbl. *Biophys. J.* **110**, 2630–2641 (2016).
45. Oury, J. et al. Mechanism of disease and therapeutic rescue of Dok7 congenital myasthenia. *Nature* **595**, 404–408 (2021).
46. Martinez-Pena y Valenzuela, I. & Akaaboune, M. The metabolic stability of the nicotinic acetylcholine receptor at the neuromuscular junction. *Cells* **10**, 358 (2021).
47. Zhang, Z., Qin, Y. W., Brewer, G. & Jing, Q. MicroRNA degradation and turnover: regulating the regulators. *Wiley Interdiscip. Rev. RNA* **3**, 593–600 (2012).
48. Besser, J. et al. MiRNA-1/133a clusters regulate adrenergic control of cardiac repolarization. *PLoS One* **9**, e113449 (2014).
49. Yu, Z. & Hecht, N. B. The DNA/RNA-binding protein, translin, binds microRNA122a and increases its in vivo stability. *J. Androl.* **29**, 572–579 (2008).
50. Roberts, T. C. The MicroRNA biology of the mammalian nucleus. *Mol. Ther. Nucleic Acids* **3**, e188 (2014).
51. Williams, A. H. et al. MicroRNA-206 delays ALS progression and promotes regeneration of neuromuscular synapses in mice. *Science* **326**, 1549–1554 (2009).
52. Liu, N. et al. microRNA-206 promotes skeletal muscle regeneration and delays progression of Duchenne muscular dystrophy in mice. *J. Clin. Invest* **122**, 2054–2065 (2012).
53. Horak, M., Novak, J. & Bienertova-Vasku, J. Muscle-specific microRNAs in skeletal muscle development. *Dev. Biol.* **410**, 1–13 (2016).
54. Yoshida, T. et al. Evaluation of off-target effects of gapmer antisense oligonucleotides using human cells. *Genes Cells* **24**, 827–835 (2019).
55. Baumann, V. & Winkler, J. miRNA-based therapies: Strategies and delivery platforms for oligonucleotide and non-oligonucleotide agents. *Future Med Chem.* **6**, 1967–1984 (2014).
56. Stenvang, J., Petri, A., Lindow, M., Obad, S. & Kauppinen, S. Inhibition of microRNA function by anti-miR oligonucleotides. *Silence* **3**, 1 (2012).
57. Lepper, C. & Fan, C. M. Inducible lineage tracing of Pax7-descendant cells reveals embryonic origin of adult satellite cells. *Genesis* **48**, 424–436 (2010).
58. Balboa, D. et al. Conditionally stabilized dCas9 activator for controlling gene expression in human cell reprogramming and differentiation. *Stem Cell Rep.* **5**, 448–459 (2015).
59. Ran, F. A. et al. Genome engineering using the CRISPR-Cas9 system. *Nat. Protoc.* **8**, 2281–2308 (2013).
60. Hall, A. B. et al. Requirements for Vav guanine nucleotide exchange factors and Rho GTPases in FcγR3A- and complement-mediated phagocytosis. *Immunity* **24**, 305–316 (2006).
61. Schutt, C. et al. Linc-MYH configures INO80 to regulate muscle stem cell numbers and skeletal muscle hypertrophy. *EMBO J.* **39**, e105098 (2020).
62. Wilkinson D. G. *In Situ Hybridization: A Practical Approach*. Oxford University Press (1992).

63. Subramanian, A. et al. Gene set enrichment analysis: a knowledge-based approach for interpreting genome-wide expression profiles. *Proc. Natl Acad. Sci. USA* **102**, 15545–15550 (2005).
64. Lin, W. et al. Distinct roles of nerve and muscle in postsynaptic differentiation of the neuromuscular synapse. *Nature* **410**, 1057–1064 (2001).
65. Billing, A. M., Ben Hamidane, H. & Graumann, J. Quantitative proteomic approaches in mouse: stable isotope incorporation by metabolic (SILAC) or chemical labeling (reductive dimethylation) combined with high-resolution mass spectrometry. *Curr. Protoc. Mouse Biol.* **5**, 1–20 (2015).
66. Boersema, P. J., Raijmakers, R., Lemeer, S., Mohammed, S. & Heck, A. J. Multiplex peptide stable isotope dimethyl labeling for quantitative proteomics. *Nat. Protoc.* **4**, 484–494 (2009).
67. Rappsilber, J., Ishihama, Y. & Mann, M. Stop and go extraction tips for matrix-assisted laser desorption/ionization, nanoelectrospray, and LC/MS sample pretreatment in proteomics. *Anal. Chem.* **75**, 663–670 (2003).
68. Shevchenko, A., Tomas, H., Havlis, J., Olsen, J. V. & Mann, M. In-gel digestion for mass spectrometric characterization of proteins and proteomes. *Nat. Protoc.* **1**, 2856–2860 (2006).
69. Kiweler, M., Looso, M. & Graumann, J. MARMoSET - Extracting Publication-ready Mass Spectrometry Metadata from RAW Files. *Mol. Cell Proteom.* **18**, 1700–1702 (2019).
70. Cox, J. & Mann, M. MaxQuant enables high peptide identification rates, individualized p.p.b.-range mass accuracies and proteome-wide protein quantification. *Nat. Biotechnol.* **26**, 1367–1372 (2008).
71. Cox, J. et al. Andromeda: A peptide search engine integrated into the MaxQuant environment. *J. Proteome Res.* **10**, 1794–1805 (2011).
72. Cox, J. et al. Accurate proteome-wide label-free quantification by delayed normalization and maximal peptide ratio extraction, termed MaxLFQ. *Mol. Cell Proteom.* **13**, 2513–2526 (2014).
73. UniProt C. UniProt: a worldwide hub of protein knowledge. *Nucleic Acids Res* **47**, D506–D515 (2019).
74. Ritchie, M. E. et al. limma powers differential expression analyses for RNA-sequencing and microarray studies. *Nucleic Acids Res* **43**, e47 (2015).

Acknowledgements

We would like to thank Kerstin Richter, Sylvia Thomas, Susanne Kreutzer, Sonja Krueger and Silvia Jeratsch for technical assistance. We thank Ann Atzberger and Johannes Graumann for FACS service and mass spectrometry analysis service, respectively. We thank Ulrich Gärtner and Gerhard Kripp for electron microscopy. This work was supported by the Max-Planck-Society, the Deutsche Forschungsgemeinschaft (D.F.G.) RTG 2355 (T.Boe) and the Transregional Collaborative Research Center TRR267 (T.Boe, T.B.) and TRR81 (T.B.) as well as by the Excellence Cluster Cardio-Pulmonary Institute (C.P.I.) and the German Center for Cardiovascular Research.

Author contributions

I.K. and T.Boe conceived and designed experiments. I.K. performed most of the experiments, C.S. contributed to experiments on adult mouse motor function and histology, T.G. contributed to experiments on Mu.S.C. differentiation. I.K., T.Boe, and C.S. analyzed the data and prepared figures. T.B. and T.Boe participated in data analysis, discussions and provided advice. I.K., T.Boe, and T.B. wrote the manuscript.

Funding

Open Access funding enabled and organized by Projekt DEAL.

Competing interests

The authors declare no competing interests.

Additional information

Supplementary information The online version contains supplementary material available at <https://doi.org/10.1038/s41467-022-30778-7>.

Correspondence and requests for materials should be addressed to Thomas Boettger or Thomas Braun.

Peer review information *Nature Communications* thanks Lin Mei, Markus Ruegg, and the other anonymous reviewers for their contribution to the peer review of this work. Peer reviewer reports are available.

Reprints and permission information is available at <http://www.nature.com/reprints>

Publisher's note Springer Nature remains neutral with regard to jurisdictional claims in published maps and institutional affiliations.



Open Access This article is licensed under a Creative Commons Attribution 4.0 International License, which permits use, sharing, adaptation, distribution and reproduction in any medium or format, as long as you give appropriate credit to the original author(s) and the source, provide a link to the Creative Commons license, and indicate if changes were made. The images or other third party material in this article are included in the article's Creative Commons license, unless indicated otherwise in a credit line to the material. If material is not included in the article's Creative Commons license and your intended use is not permitted by statutory regulation or exceeds the permitted use, you will need to obtain permission directly from the copyright holder. To view a copy of this license, visit <http://creativecommons.org/licenses/by/4.0/>.

© The Author(s) 2022